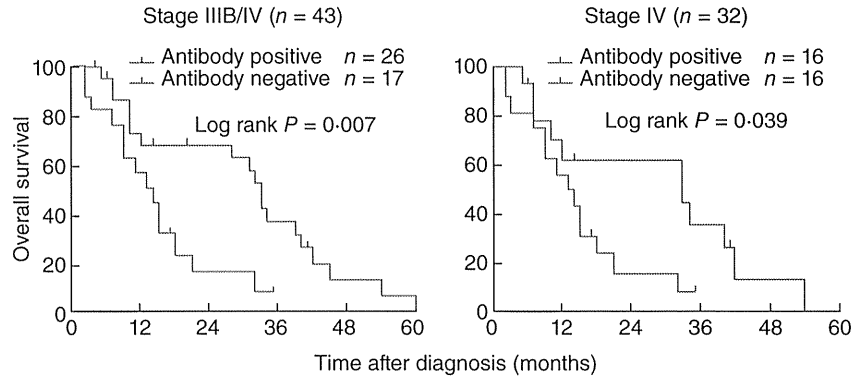

Stage	Overall survival	Antibody		*P*-value
		Positive	Negative	
Stage IIIB/IV	Median, month	33·0	14·0	0·007
	95% CI	30·3–35·7	8·2–19·8	
Stage IV	Median, month	33·0	13·0	0·039
	95% CI	0–66·1	7·1–18·9	

Fig. 1. Kaplan–Meier survival plots of XAGE-1b antigen-positive advanced lung adenocarcinoma patients as a function of XAGE-1b antibody.

suggest that the association of γ and κ chains in IgG antibodies directed against XAGE-1b might not be random. Only γ and κ chains carrying specific GM and KM allotypes might form a paratope with the necessary quaternary structure for an effective recognition of the XAGE-1b epitopes. Non-random pairing of heavy and light chains has been reported in experimental animals [22,23].

As mentioned previously, the XAGE-1b antigen is highly immunogenic and, therefore, an excellent vaccine candidate for active immunotherapy. In XAGE-1b antibody-positive patients, specific T cell responses were also frequently observed [17]. If the results presented here are confirmed in an independent study, they could aid in identifying subjects (GM 1,2,17 21) who are more likely to benefit from XAGE-1b-based vaccines. For those with the non-responder (GM 1,17 21) phenotype, XAGE-1b could be fused with appropriate adjuvants, such as heat shock proteins or flagellin, to overcome the allotypic restriction in immune responsiveness. It is relevant to note that antibody responses to certain heat shock proteins as well as to flagellin are also influenced by GM genotypes [24,25], making it conceivable to formulate a fusion XAGE-1b–heat shock protein/flagellin vaccine that could potentially generate high antibody responses in the majority of the population. Identification of the natural responders/non-responders to XAGE-1b would also be helpful in the proper evaluation of any future vaccine efficacy trials.

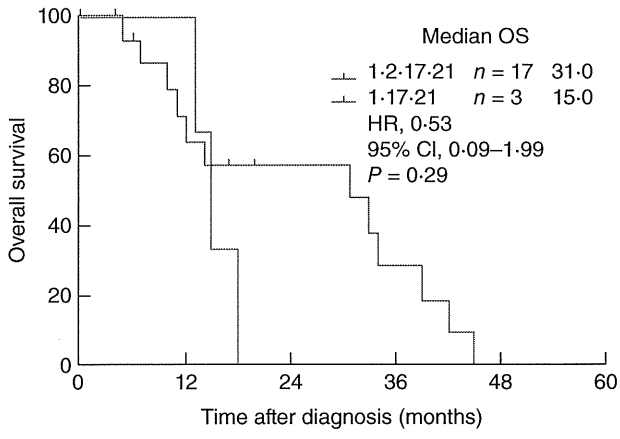

Fig. 2. Kaplan–Meier survival plots of XAGE-1b antigen-positive stage IIIB/IV lung adenocarcinoma patients as a function of GM 1,2,17 21 and GM 1,17 21 phenotypes.

Associations observed in this report can also be explained by postulating as-yet unidentified immune response genes for XAGE-1b whose alleles might be in linkage disequilibrium with those of GM and KM loci.

Although the results reported here are statistically significant, they could also be the result of chance fluctuations, as the *P*-values for the associations were not adjusted for multiple testing. Such adjustment is controversial [26], and in the present investigation would be overly punitive, as the multiple tests performed are not independent due to significant linkage disequilibrium in the GM gene complex. This is the first study of its kind, and needs to be replicated and extended by independent investigations.

It is relevant to point out that the highly significant GM phenotype–lung cancer association that was reported more than three decades ago [8] has not been confirmed or refuted by modern genome-wide association studies (GWAS) of this malignancy [27]. One contributing factor for this omission might be the absence of GM gene probes in most genotyping platforms. GWAS are assumed to be able to detect/tag all single nucleotide polymorphisms (SNPs) in the genome whose frequency is at least 5%. This, however, is not true. Most GM alleles are common within a racial group (some with allele frequency >70%), but the *IGHG* gene segments harbouring them are highly homologous and apparently not amenable to the high-throughput genotyping technology used in GWAS. Because these genes

were not typed in the HapMap or the 1000 Genomes projects, they cannot be imputed or tagged (through linkage disequilibrium) by any SNPs that are included in the genotyping platforms. Therefore, a candidate gene approach would be necessary to confirm/refute the findings reported here.

It is hoped that these results, coupled with those identifying the *IGKC* gene as a strong prognostic marker in human solid tumours [18], would inspire large-scale studies to determine conclusively the contribution of Ig GM and KM alleles in humoral immunity to XAGE-1b. It would also be of interest to investigate the role of these determinants in immunity to NY-ESO-1, a prototype cancer-testis antigen. Results from such investigations would be extremely valuable in devising novel immunotherapeutic interventions in patients with lung adenocarcinoma.

Acknowledgements

The study was supported by Project for Development of Innovative Research on Cancer Therapeutics of Ministry of Education, Culture Sports Science and Technology of Japan.

Disclosure

The authors have no conflicts of interest to declare.

References

1 Grubb R. Advances in human immunoglobulin allotypes. Exp Clin Immunogenet 1995; **12**:191–7.
2 Pandey JP, Li Z. The forgotten tale of immunoglobulin allotypes in cancer risk and treatment. Exp Hematol Oncol 2013; **2**:6.
3 Pandey JP, Kistner-Griffin E, Iwasaki M *et al.* Genetic markers of immunoglobulin G and susceptibility to breast cancer. Hum Immunol 2012; **73**:1155–8.
4 Morell A, Scherz R, Käser H, Skvaril F. Evidence for an association between uncommon Gm phenotypes and neuroblastoma. Lancet 1977; **1**:23–4.
5 Ilić V, Milosević-Jovcić N, Marković D *et al.* A biased Gm haplotype and Gm paraprotein allotype in multiple myeloma suggests a role for the Gm system in myeloma development. Int J Immunogenet 2007; **34**:119–25.
6 Pandey JP, Johnson AH, Fudenberg HH *et al.* HLA antigens and immunoglobulin allotypes in patients with malignant melanoma. Hum Immunol 1981; **2**:185–90.
7 Pandey JP, Ebbesen P, Bülow S *et al.* IgG heavy-chain (Gm) allotypes in familial polyposis coli. Am J Hum Genet 1986; **39**:133–6.
8 Nakao Y, Matsumoto H, Miyazaki T *et al.* Immunoglobulin G heavy-chain allotypes as possible genetic markers for human cancer. J Natl Cancer Inst 1981; **67**:47–50.
9 Pandey JP, Namboodiri AM, Kistner-Griffin E. IgG and FcγR genotypes and humoral immunity to mucin 1 in prostate cancer. Hum Immunol 2013; **74**:1030–33.
10 Pandey JP, Nietert PJ, Mensdorff-Pouilly S *et al.* Immunoglobulin allotypes influence antibody responses to mucin 1 in patients with gastric cancer. Cancer Res 2008; **68**:4442–46.
11 Pandey JP, Nietert PJ, Klaamas K *et al.* A genetic variant of immunoglobulin γ2 is strongly associated with natural immunity to mucin 1 in patients with breast cancer. Cancer Immunol Immunother 2009; **58**:2025–29.
12 Pandey JP, Namboodiri AM, Kurtenkov O *et al.* Genetic regulation of antibody responses to human epidermal growth factor receptor 2 (HER-2) in breast cancer. Hum Immunol 2010; **71**:1124–27.
13 Pandey JP, Namboodiri AM, Kistner-Griffin E *et al.* Racially restricted contribution of immunoglobulin Fcγ and Fcγ receptor genotypes to humoral immunity to human epidermal growth factor receptor 2 in breast cancer. Clin Exp Immunol 2013; **171**:273–7.
14 Pandey JP, Shannon BT, Tsang KY *et al.* Heterozygosity at Gm loci associated with humoral immunity to osteosarcoma. J Exp Med 1982; **155**:1228–32.
15 Ali Eldib AM, Ono T, Shimono M *et al.* Immunoscreening of a cDNA library from a lung cancer cell line using autologous patient serum: identification of XAGE-1b as a dominant antigen and its immunogenicity in lung adenocarcinoma. Int J Cancer 2004; **108**:558–63.
16 Nakagawa K, Noguchi Y, Uenaka A *et al.* XAGE-1 expression in non-small cell lung cancer and antibody response in patients. Clin Cancer Res 2005; **11**:5496–503.
17 Ohue Y, Eikawa S, Okazaki N *et al.* Spontaneous antibody, and CD4 and CD8 T-cell responses against XAGE-1b (GAGED2a) in non-small cell lung cancer patients. Int J Cancer 2012; **131**:E649–58.
18 Schmidt M, Hellwig B, Hammad S *et al.* A comprehensive analysis of human gene expression profiles identifies stromal immunoglobulin kappa C as a compatible prognostic marker in human solid tumors. Clin Cancer Res 2012; **18**:2695–704.
19 Schanfield MS, van Loghem E. Human immunoglobulin allotypes. In: Weir DM, ed. Handbook of experimental immunology. Boston, MA: Blackwell, 1986:94.1–18.
20 Casadevall A, Pirofski L-A. A new synthesis for antibody-mediated immunity. Nat Immunol 2012; **13**:21–8.
21 Morahan G, Berek C, Miller JFAP. An idiotypic determinant formed by both immunoglobulin constant and variable regions. Nature 1983; **301**:720–22.
22 Czerwinski M, Siemaszko D, Siegel DL *et al.* Only selected light chains combine with a given heavy chain to confer specificity for a model glycopeptide antigen. J Immunol 1998; **160**:4406–17.
23 Primi D, Drapier AM, Cazenave PA. Highly preferential VH–VL pairing in normal B cells results in antigen-independent selection of the available repertoire. J Immunol 1987; **138**:1607–12.
24 Pandey JP, Prohászka Z, Veres A *et al.* Epistatic effects of genes encoding immunoglobulin GM allotypes and interleukin-6 on the production of autoantibodies to 60- and 65-kDa heat-shock proteins. Genes Immun 2004; **5**:68–71.
25 Pandey JP. Comment on 'Flagellin as an adjuvant: cellular mechanisms and potential'. J Immunol 2011; **186**:1299.
26 Perneger TV. What's wrong with Bonferroni adjustments. BMJ 1998; **316**:1236–38.
27 Shiraishi K, Kunitoh H, Daigo Y *et al.* A genome-wide association study identifies two new susceptibility loci for lung adenocarcinoma in the Japanese population. Nat Genet 2012; **44**:900–3.

Published online 27 September 2014

Nucleic Acids Research, 2014, Vol. 42, No. 19 ***11903–11911***
doi: 10.1093/nar/gku881

HSP90α plays an important role in piRNA biogenesis and retrotransposon repression in mouse

Tomoko Ichiyanagi[1,2,†], Kenji Ichiyanagi[2,†], Ayako Ogawa[2], Satomi Kuramochi-Miyagawa[3,4], Toru Nakano[3,4], Shinichiro Chuma[5], Hiroyuki Sasaki[2] and Heiichiro Udono[1,*]

[1]Department of Immunology, Okayama University Graduate School of Medicine, Dentistry, and Pharmaceutical Sciences, Kita-ku, Okayama 700-8558, Japan, [2]Division of Epigenomics and Development, Medical Institute of Bioregulation, Kyushu University, Higashi-ku, Fukuoka 812-8582, Japan, [3]Department of Pathology, Medical School and Graduate School of Frontier Biosciences, Osaka University, Suita, Osaka 565-0871, Japan, [4]CREST, Japan Science and Technology Agency (JST), Saitama 332-0012, Japan and [5]Department of Development and Differentiation, Institute for Frontier Medical Sciences, Kyoto University, Sakyo-ku, Kyoto 606-8507, Japan

Received July 8, 2014; Revised September 07, 2014; Accepted September 13, 2014

ABSTRACT

HSP90, found in all kingdoms of life, is a major chaperone protein regulating many client proteins. We demonstrated that HSP90α, one of two paralogs duplicated in vertebrates, plays an important role in the biogenesis of fetal PIWI-interacting RNAs (piRNA), which act against the transposon activities, in mouse male germ cells. The knockout mutation of *Hsp90α* resulted in a large reduction in the expression of primary and secondary piRNAs and mislocalization of MIWI2, a PIWI homolog. Whereas the mutation in *Fkbp6* encoding a co-chaperone reduced piRNAs of 28–32 nucleotides in length, the *Hsp90α* mutation reduced piRNAs of 24–32 nucleotides, suggesting the presence of both FKBP6-dependent and -independent actions of HSP90α. Although DNA methylation and mRNA levels of L1 retrotransposon were largely unchanged in the *Hsp90α* mutant testes, the L1-encoded protein was increased, suggesting the presence of post-transcriptional regulation. This study revealed the specialized function of the HSP90α isofom in the piRNA biogenesis and repression of retrotransposons during the development of male germ cells in mammals.

INTRODUCTION

Heat-shock protein 90 (HSP90), the most abundant protein in mammalian cells, is a chaperone that stabilizes the conformation of >200 client proteins in various physiological pathways, thereby maintaining cellular homeostasis (1,2). In mammals, there are two cytosolic HSP90 isoforms encoded by distinct genes, *Hsp90aa1* (HSP86; HSP90α) and *Hsp90ab1* (HSP84; HSP90β) sharing 86% similarity in amino acid sequences, as well as HSP90 family proteins localized in the mitochondria and endoplasmic reticulum. For simplicity, we refer to *Hsp90aa1* and *Hsp90ab1* as *Hsp90α* and *Hsp90β*, respectively. Although *Hsp90β* is ubiquitously expressed (constitutive type), *Hsp90α* expression is increased in response to various stresses (inducible type), and its expression is more tissue-specific at the steady state, being relatively higher in the testes and brain (3–5). Whether these HSP90 proteins have specific functions remains unclear.

Recently, plant and insect HSP90 proteins were implicated in the biogenesis of three major classes of small RNAs: small interfering RNA (siRNA), microRNA (miRNA) and PIWI-interacting RNA (piRNA). In insects and plants, the ATPase activities of HSP90 and HSP70 are indispensable for the formation of the pre-RNA-induced silencing complex (pre-RISC), in which double-stranded RNA precursors of siRNA and miRNA are loaded onto Argonaute proteins (6–8). In cultured human cells, however, chemical inhibition of HSP90 proteins does not affect miRNA expression, although Argonaute-2 is mislocalized (9). In animal gonads, PIWI-clade Argonaute proteins (Piwi, Aub and Ago3 in flies and MILI, MIWI and MIWI2 in mice) play a principal role in the generation of piRNAs, germline-specific small RNAs typically 24–33 nucleotides (nt) in length that counteract the transposon activities (10). In flies, Hsp90 has been implicated in piRNA production (11,12), and its co-chaperone, Hop, regulates Piwi phosphorylation and thus piRNA production (12). Moreover, silkworm Hsp90 participates in the loading of piRNA precursors onto Piwi (13). Another Hsp90 co-chaperone, Shutdown, is important for piRNA production in flies (14), and its mouse ortholog, FKBP6, has been proposed to facilitate the recycling of PIWI proteins in piRNA biogenesis

*To whom correspondence should be addressed. Tel: +81 86 235 7187; Fax: +81 86 235 7193; Email: udono@cc.okayama-u.ac.jp
†The authors wish it to be known that, in their opinion, the first two authors should be regarded as Joint First Authors.

(15). However, whether HSP90 plays a role in piRNA biogenesis in mice and other vertebrate species remains unknown. Studies on the role of the mouse HSP90 proteins in piRNA biogenesis have been hindered by the presence of two *Hsp90* genes in mice versus a single gene in insects. *Hsp90α* knockout (KO) mice are viable, presumably because of the presence of functional *Hsp90β*. However, we revealed that KO males are infertile due to a failure in spermatogenesis (16,17), suggesting that *Hsp90α* plays a role in spermatogenesis that cannot be replaced by *Hsp90β*. In this study, we investigated piRNA biogenesis in *Hsp90α* KO mice and revealed a specific function of HSP90α in the piRNA-based host-defense system against transposons in mice.

MATERIALS AND METHODS

Animals

The *Hsp90α* and *Mitopld* KO strains were described by Kajiwara *et al.* (17) and Watanabe *et al.* (18), respectively.

Antibodies

Polyclonal antibodies to HSP86 (HSP90α) and HSP84 (HSP90β) were purchased from Thermo Scientific (PA3–013, RB-118). For immunostaining, polyclonal antibodies against MILI (PIWIL2), MIWI2 (PIWIL4) and WDR77 were purchased from Abcam. Anti-TDRD1 and TDRD9 polyclonal antibodies and anti-MIWI2 polyclonal antibody for immunoprecipitation were made by S. C. (Kyoto University) and S. K.-M. (Osaka University), respectively. Anti-L1 ORF polyclonal antibody and *Mael* KO testes lysate were generous gifts from Dr A. Bortvin (Carnegie Institute) (19). Anti-mono and dimethyl arginine monoclonal antibody (7E6) used in western blot analysis was obtained from Abcam.

Oligonucleotides

The sequences of oligonucleotides used in this study are listed in Supplementary Table S1.

Immunofluorescence detection of protein localization

E16.5–18.5 testes were embedded in OCT compound and snap-frozen in liquid nitrogen or isopentane cooled in liquid nitrogen. Cryosections were cut at 7–10-μm thickness and air-dried. The sections were fixed for 10 min in 4% PFA at 4°C, washed with PBS, permeabilized in PBS with 0.5% Triton X-100 for 30 min at room temperature, and blocked in PBS with 0.1% Triton X-100 and 1% BSA for 30 min at room temperature. Primary antibodies were incubated overnight at 4°C. Slides were washed and incubated with Alexa Fluor 488-labeled secondary antibody for 2–3 h at room temperature. The sections were mounted with SlowFade Gold Antifade Reagent with DAPI (Life Technologies) and observed by fluorescence microscopy.

Small RNA sequencing analysis

Total RNA was extracted from wild-type (WT) and *Hsp90α* KO testes on E16.5 (20 testes for each condition) by Isogen (Toyobo, Japan) and used to create a small RNA library using the TruSeq Small RNA Library Preparation Kit (Illumina). The libraries were sequenced on MiSeq (Illumina) via 50-bp single-end sequencing. After clipping the adaptor sequence, sequence reads of more than 10 bp were mapped to cellular RNA and miRNA sequences in miRBase (20) by SeqMap (21). Unmapped sequences were then mapped to the mouse genome sequence, allowing no mismatch, and the mouse transposon sequences obtained from RepBase (22), allowing 2-bp mismatches. For piRNA cluster-derived RNAs, the sequences uniquely mapped to the fetal piRNA clusters (23) were analyzed.

The small RNA sequencing data were obtained from Gene Expression Omnibus (GEO) for *Fkbp6* KO and its WT control (GSE39203). These data and our published data for *Mili* KO, *Miwi2* KO and their WT control (GSE20327) were analyzed using the aforementioned reference sequences.

Immunoprecipitation and western blotting

Three pairs of E16.5 testes were lysed in lysis buffer [20 mM HEPES pH 7.5, 150 mM NaCl, 2.5 mM $MgCl_2$, 0.1% Nonidet P-40 (NP40), 1 mM DTT, protease inhibitor cocktail (Nacalai, Japan)] on ice using a Dounce homogenizer, and the lysate was cleared by centrifugation at 17,800 × g for 15 min at 4°C. The lysate was incubated with anti-MIWI2 antibody overnight at 4°C, following which Protein A/G PLUS-Agarose was added to collect the antibody and protein complexes. The agarose beads were washed four times with wash buffer (25 mM Tris-HCl pH 7.5, 150 mM NaCl, 2.5 mM $MgCl_2$, 0.05% NP40 supplemented with 1 mM DTT, protease inhibitor cocktail). Immunoprecipitants were eluted in sodium dodecyl sulphate (SDS) sample buffer and run on an SDS-polyacrylamide gel electrophoresis gel. Western blotting was performed as described previously (24).

Methylation-sensitive Southern blotting

The genomic DNAs of WT or *Hsp90α* KO testes at P14 (5 μg each) were digested by MspI (methylation insensitive) or HpaII (methylation sensitive) and run on a 0.8% agarose gel. DNAs were then transferred to a Hybond XL membrane (GE Healthcare), hybridized with a ^{32}P-labeled L1 probe (25) at 42°C for 20 h and washed four times with wash buffer (2× SSC, 0.1% SDS) at 42°C. The radioactivities on the membrane were detected on a BAS2500 analyzer (Fujifilm, Japan).

Northern blotting

Total RNA (10 μg each) was run on a 15% polyacrylamide gel, transferred to a Hybond XL membrane using a semi-dry method (100 mA, 2 h) and cross-linked by UV. The membrane was hybridized against radioactive probes at 40°C overnight and washed four times in wash buffer (2× SSC, 0.1% SDS). The L1 (piR-1831) and Intracisternal A particle (IAP) (piR-4868) probes used were described previously (25).

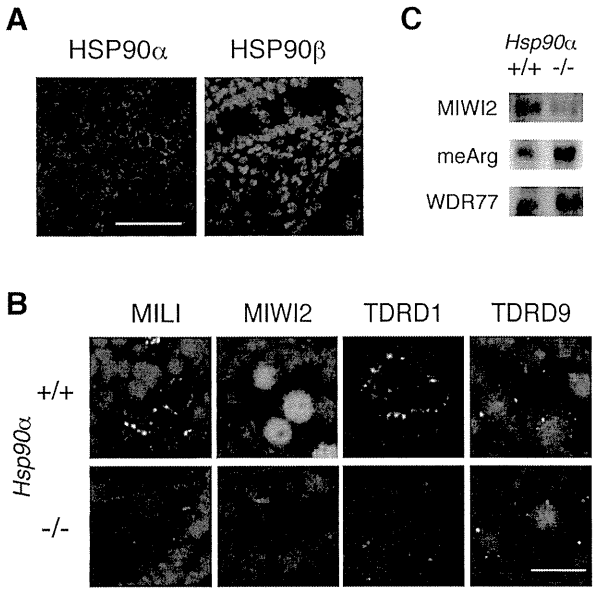

Figure 1. The *Hsp90α* mutation affected the localization but not the arginine methylation of MIWI2. (**A**) Immunofluorescence staining of HSP90α (green; left) or HSP90β (green; right) in WT E18.5 testes. Nuclei were counter-stained with DAPI (blue). (**B**) Localization of piRNA-related proteins (green) in E18.5 WT (top) and Hsp90α KO (bottom) testis. Bars: *A*: 50 μm *B*: 20 μm. (**C**) MIWI2 was immunoprecipitated from the E16.5 testes of WT or Hsp90α KO mice and subjected to western blotting. Immunoprecipitants were blotted for MIWI2 (top), methyl-arginine (middle) and WDR77 (bottom). See also Supplementary Figure S1.

Germ cell preparation and bisulfite sequencing

Germ cells were purified by fluorescence activated cell sorting. Prospermatogonia were isolated from P0 testes of mice carrying an Oct4-EGFP transgene. Spermatocytes were isolated from P17 testes as described previously (26). Genomic DNA was isolated by standard procedure and used for bisulfite sequencing as described previously (27). For each germ cell preparation, the cell purity was validated by confirming the percentages of DNA methylation in the Lit1 differentially methylated region, which is completely unmethylated in male germ cells and 50% methylated in somatic cells.

RESULTS

Hsp90α mutation affects the localization of MIWI2, a PIWI protein

Immunofluorescence analysis revealed that HSP90α is specifically expressed in germ cells (prospermatogonia) in the testis on embryonic day 16.5 (E16.5), whereas HSP90β is expressed in both somatic and germ cells, suggesting a germ cell-specific function of HSP90α (Figure 1A). The prospermatogonia produce piRNAs at this developmental stage, and a deficiency in the biogenesis of fetal piRNAs in animals with mutations in piRNA-related genes such as *Mili*, *Miwi2*, *Tdrd1*, *Tdrd9*, *Mov10l1*, *Maelstrom* and *Mitopld* leads to a failure in spermatogenesis (10). We therefore investigated whether subcellular localization and/or expression levels of piRNA-related proteins are affected by the *Hsp90α* KO mutation in E18.5 testes. Proteins involved in piRNA biogenesis co-localize at granules around the periphery of the nucleus. MILI, one of the two PIWI proteins expressed in prospermatogonia, and TDRD1 localize at cytoplasmic granules at the periphery of nucleus, called pi-bodies, whereas the other PIWI protein MIWI2 as well as TDRD9 and MAELSTROM localizes at different cytoplasmic granules around the nucleus, called piP-bodies (28). MIWI2 and TDRD9 also localize in the nucleus, which is thought to be important for piRNA-targeted DNA methylation (25,29). In *Hsp90α* KO mice, MILI expression and localization were unaffected (Figure 1B and Supplementary Figure S1A). However, we detected an obvious difference in MIWI2 localization. Although MIWI2 localizes both at perinuclear granules and in the nucleus in the WT germ cells, nuclear staining was significantly decreased in *Hsp90α* KO germ cells (Figure 1B), although some staining still remained in nuclei. At the mRNA level, the *Miwi2* expression was not affected in *Hsp90α* KO testes at E16.5 (Supplementary Figure S1B).

Because MIWI2 interacts with TDRD9, a Tudor domain-containing protein (25,30), we investigated TDRD9 expression in *Hsp90α* KO mice as well as the expression of another Tudor protein, TDRD1, which interacts with MILI. The localization of TDRD9 and TDRD1 was unchanged in *Hsp90α* KO mice (Figure 1B). The expression and localization of the other proteins involved in fetal piRNA biogenesis, MAELSTROM and MOV10L1, were also unaffected in *Hsp90α* KO mice (Supplementary Figure S1C).

MIWI2 was methylated at arginines in WT and *Hsp90α* KO testes

The Tudor domains in various proteins specifically bind to methylated arginine residues (31), and it has been postulated that the MIWI2-TDRD9 interaction depends on the methylation of arginine residue(s) in MIWI2 at its RA/RG motifs, which is likely catalyzed by an arginine methyltransferase, PRMT5 (32,33). PRMT5 is a client protein of HSP90, and PRMT5 and HSP90α were found to interact with MIWI2 (32). Moreover, chemical inhibition of HSP90 activity severely diminishes the stability of the PRMT5 protein in cultured cells (34). Therefore, we investigated the arginine methylation of MIWI2 in WT and *Hsp90α* KO mice. For this purpose, MIWI2 was first immunoprecipitated in whole cell lysates of E16.5 testes, and the precipitants were analyzed by western blotting against an anti-methylarginine antibody. We detected an arginine-methylated protein in the WT preparation that co-migrated with MIWI2 in the gel (Figure 1C), suggesting that MIWI2 is indeed methylated at arginine(s) in prospermatogonia. The level of arginine methylation was comparable between WT and KO preparations, suggesting that the arginine methylation of MIWI2 is not disturbed in *Hsp90α* KO mice. Presumably, HSP90β may facilitate PRMT5 activity. WDR77, a co-factor of PRMT5, was detected in the MIWI2-IP fraction of *Hsp90α* KO testes, and the amount was similar to that of WT testes (Figure 1C).

Our results together suggest that in the absence of HSP90α, MIWI2 fails to enter the nucleus even though MIWI2 is methylated and its associated partners, TDRD9

and MAELSTROM, are properly expressed and localized. Failure in MIWI2 translocation is also observed in *Mili*, *Tdrd1*, *Tdrd12*, *Maelstrom*, *Mov10l1* and *Fkbp6* mutant mice (15,25,35–37), all of which are deficient in piRNA biogenesis to various degrees. Therefore, we analyzed small RNAs from WT and *Hsp90α* mutant testes. For comparison, we also analyzed published small RNA sequencing data for *Mili*, *Miwi2* and *Fkbp6* KO testes and their WT controls.

Hsp90α mutation displayed a remarkable decrease in fetal piRNAs

Fetal piRNAs are classified into two types: primary and secondary piRNAs. Primary piRNAs are generated from precursor RNAs transcribed from ~200 genomic regions called piRNA clusters. Transposon-derived RNAs are also the sources of the primary piRNAs. These primary piRNAs preferentially have uracil at the first position, and they are loaded onto MILI. MILI cleaves RNAs containing transposon sequences that are complementary to the primary piRNA. This generates secondary piRNAs, which preferentially have adenine at the 10th position. The secondary piRNAs are loaded onto either MILI or MIWI2 to guide the cleavage of complementary RNAs, a process called the ping-pong cycle. We therefore analyzed both types of piRNAs as well as miRNAs.

Small RNA libraries were generated from WT and *Hsp90α* KO testes at E16.5 and deeply sequenced (Figure 2A). The miRNA reads in the WT and KO libraries were comparable (83.2 and 83.9% of the total 20–23-nt RNAs, respectively). In contrast, the levels of 24–33-nt small RNAs uniquely mapped to the previously identified fetal piRNA clusters, representing primary piRNAs, were reduced by ~3-fold in the KO testes (Figure 2B and C). The levels of 24–33-nt small RNAs mapped to transposon sequences, consisting of primary and secondary piRNAs, were also reduced by ~3-fold (Figure 2D and E). Similar trends were observed in the *Fkbp6* co-chaperone mutant (Figure 2B and D; Xiol *et al.* (15)); however, the effect was larger in *Hsp90α* mutants than in *Fkbp6* mutants. The *Fkbp6* mutation reduced the expression of small RNAs in the range of 28–32 nt, the size range of MIWI2-bound piRNAs; however, it did not affect 24–27-nt RNAs, the size range of MILI-bound piRNAs (Supplementary Figure S2A). In contrast, the *Hsp90α* mutation equally suppressed the expression of 24–32-nt RNAs (Supplementary Figure S2C), suggesting the presence of both FKBP6-dependent and FKBP6-independent actions of HSP90α. In any event, these results indicate that HSP90α plays a role in the biogenesis and/or stability of piRNAs in prospermatogonia. Whereas the *Mili* mutation severely downregulates both cluster- and transposon-derived piRNAs, the *Miwi2* mutation does not reduce cluster-derived piRNAs (Figure 2B and D; Aravin *et al.* (35)). Therefore, the downregulation of both types of piRNAs in *Hsp90α* KO germ cells suggests that HSP90α affects both the activity of MIWI2 and the upstream reaction(s) in the piRNA biogenesis pathway, possibly primary piRNA biogenesis and/or stability.

To study the role of HSP90α in the piRNA pathway in more detail, we analyzed small RNAs mapped to the consensus sequence of A-type LINE-1 (L1), one of the most active retrotransposons in the mouse genome (Figure 3A). Both sense and antisense small RNA levels were reduced in the KO testes. Although this global reduction, the mapped 24–33-nt small RNAs in the KO library displayed a bias toward uracil at the first position and adenine at the 10th position as well as a 10-bp overlap between sense and antisense small RNAs (Figures 2C, E and 3B), which are the hallmarks of piRNAs generated via the ping-pong cycle. We also detected an ~3-fold reduction in the expression of piRNAs derived from Gf-type L1, another active L1 subfamily, in KO testes.

In addition to the length range of typical piRNAs, we detected a number of 19-nt small RNAs, which were positioned immediately upstream of 24–33-nt piRNAs on the same strand and were complementary to 29-nt piRNAs on the opposite strand (Figure 3A, C, and Supplementary Figure S2). Most (79%) 19-nt RNAs were associated with piRNAs that have adenine at the 10th position, and the 19-nt peak was not observed for cluster-derived small RNAs (Fig-

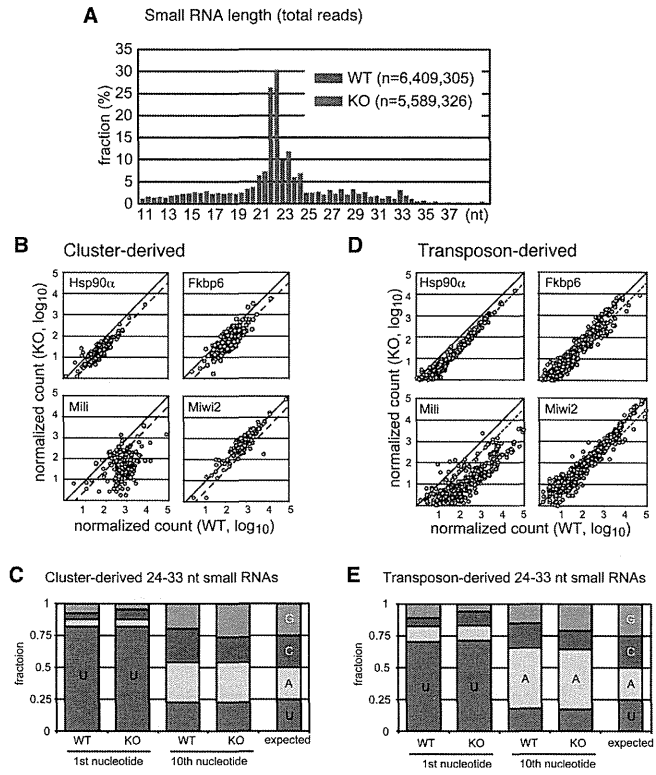

Figure 2. The *Hsp90α* KO mutation reduced both cluster- and transposon-derived small RNAs in E16.5 testes. (**A**) Length distributions of small RNA sequences in WT (blue) and *Hsp90α* KO (red) fetal testes. (**B**, **D**) Small RNA sequence reads (24–33 nt) from *Hsp90α*, *Fkbp6*, *Mili* and *Miwi2* KO testes (vertical axis), which were uniquely mapped to the fetal piRNA clusters (B) or the consensus sequences of mouse transposons (D), are plotted against those from the respective WT controls (horizontal axis). Each plot represents one of the clusters (B) or transposons (D). All sequence reads are normalized as *per million miRNA reads*. The dashed line indicates a 3-fold reduction in the KO library, and the solid line indicates no change. (**C**, **E**) The nucleotide bias at the 1st and 10th positions in the 24–33-nt small RNAs mapped to the piRNA clusters (C) and transposons (E) in WT and KO testes.

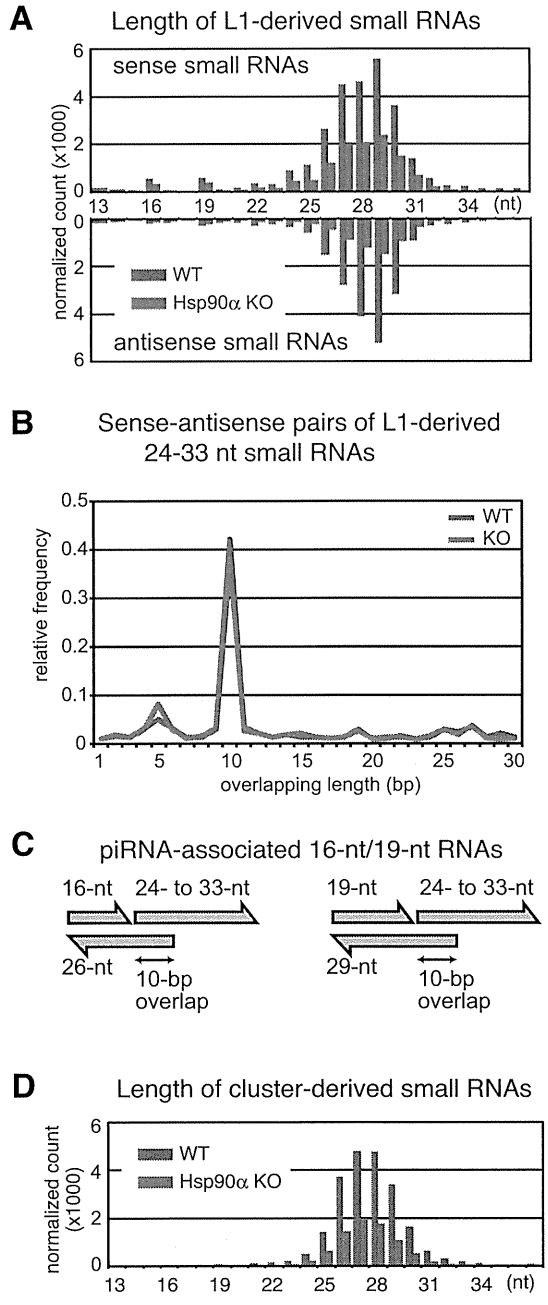

Figure 3. The *Hsp90α* KO mutation reduced L1-derived piRNAs, but not piRNA-related 16- or 19-nt small RNAs. (**A**) The length distributions of small RNAs in the WT (black) and *Hsp90α* KO (red) libraries that were mapped to the consensus sequence of the A-type L1 retrotransposon. The sense (top) and antisense (bottom) RNAs are separately presented. (**B**) Length distribution of distances between the 5′-end of 24–33-nt small RNAs mapped to the sense strand of the L1 sequence and the 5′-end of 24–33-nt small RNAs mapped to the L1 antisense strand. Blue line, WT library; red line, KO library. (**C**) Configuration of 16- and 19-nt small RNAs derived from the L1 sequence. For many 16- and 19-nt small RNAs, their end positions are 1 bp upstream of the start position of 24–33-nt small RNAs on the same strand, and their start positions are the same position as the end position of 26- and 29-nt small RNAs on the opposite strand. The two piRNA-length small RNAs overlap each other by 10 bp. See also Supplementary Figure S2 for details. (**D**) The length distributions of small RNAs in the WT (blue) and *Hsp90α* KO (red) libraries that were mapped to the previously identified piRNA clusters.

ure 3D). Therefore, these 19-nt RNAs are likely the byproducts of piRNA production via the ping-pong cycle, as has been suggested for 19-nt RNAs present in adult testes containing pachytene and prepachytene piRNAs (38,39). In addition, the presence of 16-nt byproducts was evident (Figure 3A, C and Supplementary Figure S2). The amounts of these 19- and 16-nt byproducts were only slightly reduced by the *Hsp90α* mutation. It has been reported that in cultured silkworm cells, chemical inhibition of HSP90 results in the accumulation of such 16-nt byproducts in the PIWI complex, suggesting that HSP90 facilitates the recycling of PIWI for efficient ping-pong cycling (15). In the mouse system, however, our data imply that neither RNA cleavage nor PIWI recycling is affected by HSP90α inactivation; thus, it appears more likely that HSP90α plays a role in stabilizing 24–33-nt piRNAs, such as stabilizing piRNA–protein complexes.

L1 retrotransposons are derepressed in the fetal germ cells of *Hsp90α* KO mice

The reduction of L1-derived 24–33-nt piRNAs prompted us to investigate whether the expression of this retrotransposon is misregulated in mutant prospermatogonia. Thus, we compared the expression of the L1-encoded ORF1p protein in WT and *Hsp90α* KO testes at E18.5 by immunofluorescence. The number of ORF1p-positive germ cells was significantly increased in the fetal *Hsp90α* KO testis (Figure 4A). Furthermore, western blotting of the whole testes lysates (E16.5) revealed a definite increase in ORF1p levels in the mutant testes (Figure 4B). In contrast, L1 mRNA levels were largely unchanged in these testes (Figure 4C), suggesting that the effect occurs at the post-transcriptional level. Consistently, the DNA methylation levels of the promoter sequences of A- and Gf-type L1 were largely similar between WT and KO P0 prospermatogonia (Figure 4D).

Postnatal piRNA levels derived from retrotransposons were reduced in *Hsp90α* KO mice

We also investigated the effect of the *Hsp90α* KO mutation on piRNA biogenesis and DNA methylation in postnatal germ cells. Northern blot analysis of testis RNA on postnatal day 24 (P24) against piRNA derived from IAP, another active retrotransposon, revealed a severe reduction in piRNA levels in the mutant testes (Figure 5A). The reduction of L1-derived piRNA was unclear because of smearing; however, longer RNAs were accumulated in the mutant testes, very similarly to *Mitopld* KO testes, which are deficient in piRNA production and show an increased L1 mRNA level at postnatal stages (18). These results suggest that, at the postnatal stages, L1 transcription is increased in *Hsp90α* KO testes. The DNA methylation level in the L1 promoters was partially reduced in the *Hsp90α* mutant testes at P15 when analyzed by methylation-sensitive enzyme digestion and Southern blot, although it was not as much as *Mitopld* KO testes (Figure 5B). However, when analyzed by bisulfite sequencing, the L1 promoters were normally methylated in *Hsp90α* KO meiotic germ cells (spermatocytes) at P17 (Figure 5C), as in the P0 prospermatogonia (Figure 4D). Although there might be a difference in

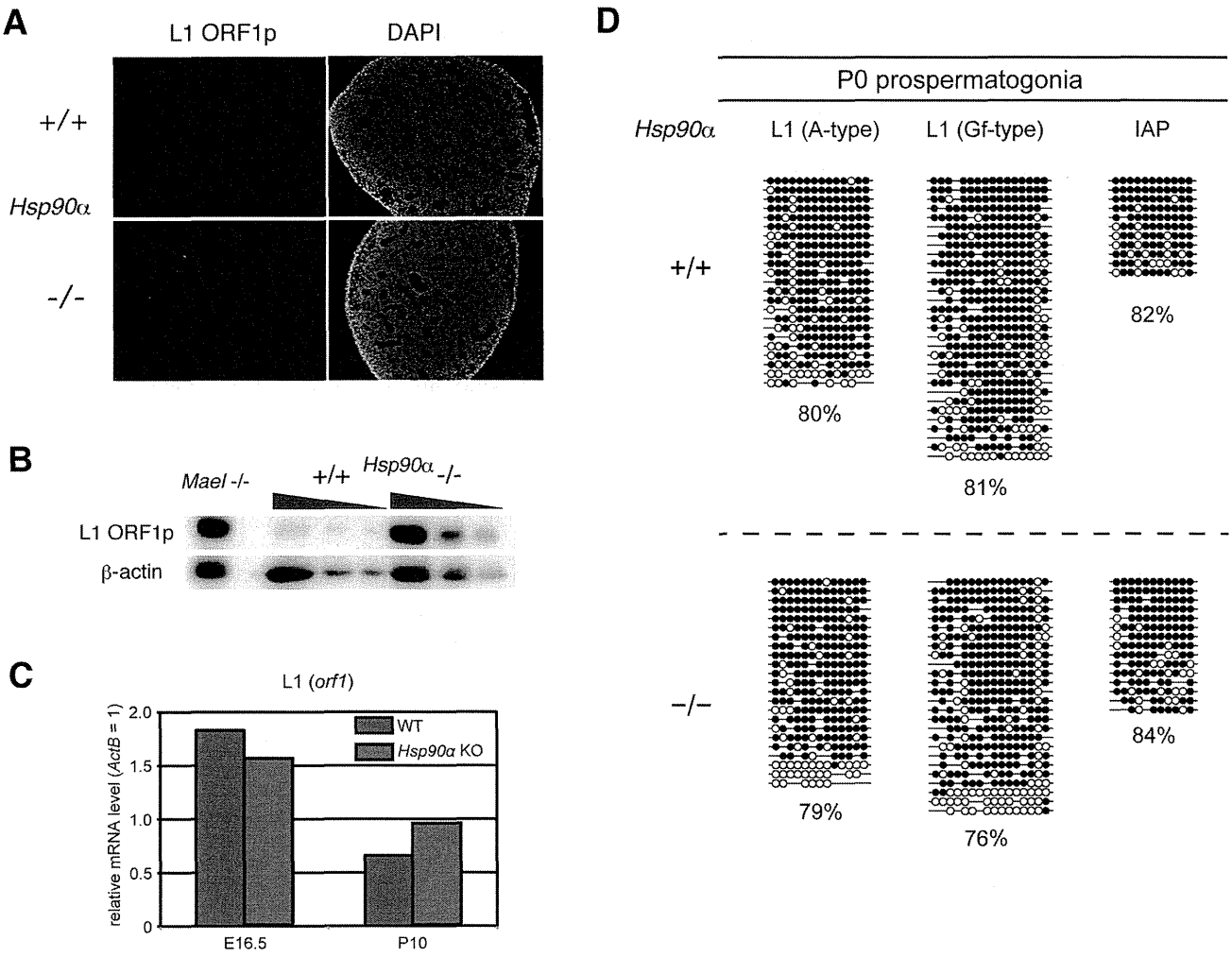

Figure 4. Increase in L1-encoded protein levels in *Hsp90α* KO testes. (**A**) Immunofluorescence detection of L1 ORF1 protein in E18.5 testes. (**B**) Western blot analysis of L1 ORF1 protein in E16.5 testes lysates. *Maelstrom* KO testis lysate (gifted from Dr A. Bortvin) was used as a positive control, and β-actin served as a loading control. (**C**) The gene expression of L1 *Orf1* in WT (blue) and *Hsp90α* KO (red) testes at E16.5 and P10 was determined by quantitative RT-PCR and normalized by the *ActB* expression level. (**D**) DNA methylation levels of retrotransposon sequences in WT and KO prospermatogonia (at P0) determined by bisulfite-PCR sequencing. Open and closed circles represent unmethylated and methylated CpG sites, respectively.

methylation in several limited loci of L1, the profound decrease in piRNA production did not affect DNA methylation of a bulk of L1 promoters.

DISCUSSION

The HSP90 proteins play a pivotal role for maintaining the integrity of cellular functions by supporting the activities of many client proteins, and this HSP90's function has been proposed to be important for the robustness of developmental pathways under genetic or environmental perturbations (i.e. canalization) (40,41). In the germ cells, maintaining the integrity of the genome and epigenome is especially important, because they convey the genetic and possibly epigenetic information to the progenies. The germline piRNA system is an efficient host defense system against the mutagenic effects of active transposons by cleaving their RNAs and epigenetically silencing their promoters. We recently revealed that Hsp90α is essential for spermatogenesis (17), and in this report, we showed that HSP90α is important for piRNA production and post-transcriptional repression of retrotransposons in mouse fetal germ cells. Several proteins indispensable for piRNA production have been identified, and there are even more proteins regulating these key proteins. The PIWI-clade Argonaute proteins, MILI and MIWI2, are the most centered in the mouse fetal piRNA system as they form complexes with primary piRNAs, cleave the transposon-derived RNAs to generate secondary piRNAs and mediate DNA methylation of transposons such as L1. The loss of HSP90α decreased both MILI- and MIWI2-bound fractions of fetal piRNAs by ~3-fold, but not completely. The remaining piRNAs showed the hallmarks of ping-pong cycle, which indicate that the RNase (slicer) activity of the PIWI protein(s) is still working in KO germ cells. Nevertheless, the decrease was enough to derepress retrotransposons.

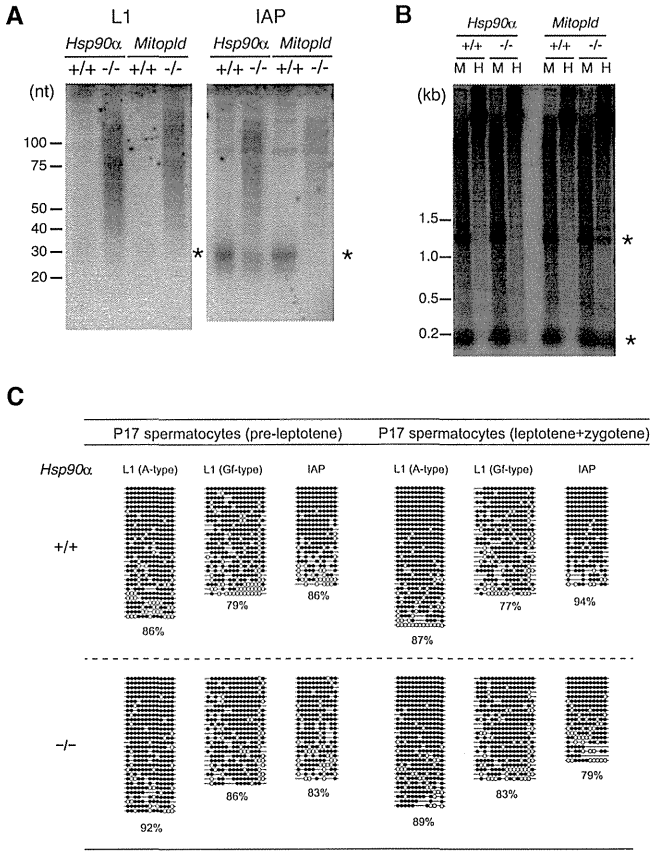

Figure 5. The expression levels of piRNA and the DNA methylation of L1 and IAP retrotransposons. (**A**) Northern blot analysis of piRNAs derived from L1 and IAP in P24 testes. Mitopld KO testes were used as a control for piRNA defects. (**B**) DNA methylation state of L1 5′-UTR was detected by Southern blot analysis of testes DNA digested by a methylation-insensitive (MspI; M) or methylation-sensitive (HpaII; H) restriction enzyme. (A, B) Asterisks indicate the expected band sizes. (**C**) DNA methylation levels of retrotransposon sequences in WT and KO spermatocytes (at P17) determined by bisulfite-PCR sequencing. Open and closed circles represent unmethylated and methylated CpG sites, respectively.

The reports on the piRNA system have been accumulating in this decade. However, the mechanisms of piRNA-mediated retrotransposon silencing are still not fully understood, especially in the series of steps: (i) the loading of MILI-generated piRNAs onto MIWI2, (ii) the translocation of MIWI2–piRNA complex into nucleus and (iii) the introduction of DNA methylation in retrotransposon promoters. TDRD9, which contains a Tudor domain recognizing methylated arginine residues, has been shown to co-localize with and binds to MIWI2 at piP-bodies and both proteins are also present in nucleus, suggesting its role in the MIWI2 translocation (25). The other PIWI proteins in postnatal germ cells, MILI and MIWI, have been shown to be methylated by an HSP90 client protein, PRMT5, which is a type II protein methyltransferase (32,33). However, it was unknown whether MIWI2 is methylated *in vivo*, although MIWI2 has the PRMT5-methylation motif and can be methylated by PRMT5 *in vitro* (32,33). Here, we showed that MIWI2 is indeed methylated in fetal germ cells. But, it is likely that the level of the MIWI2 methylation was not affected in prospermatogonia at E16.5 by the *Hsp90α* deficiency, demonstrating that the arginine methylation is not sufficient for the MIWI2 protein to translocate into nuclei. Interestingly, even with the arginine methylation of MIWI2, the subcellular localization patterns of MIWI2 and TDRD9 became different in *Hsp90α* KO germ cells; TDRD9 still can enter the nucleus in the mutant. Given the function of HSP90α in protein transport across membranes in dendritic cells (16,24), it is tempting to speculate that HSP90α may function as a chaperone for MIWI2 translocation. This prospect should be explored in future studies.

Despite the low efficiency of MIWI2 nuclear translocation and the low amount of piRNAs, the DNA methylation levels at L1 promoters were not severely affected. Therefore, the small amounts of MIWI2–piRNA complexes in the nucleus might be enough to guide *de novo* DNA methylation of the retrotransposon promoters. We showed that L1 mRNA is highly produced even in the WT fetal testes and is not extra-elevated in the *Hsp90α* KO testes. On the other hand, the amount of the L1-encoded protein was significantly elevated in the *Hsp90α* mutant testes. These features, i.e. *de novo* DNA methylation is not affected but the expression of L1 is elevated at the protein level, are very similar to the phenotype of the mutant of *Maelstrom* (28), a gene known to be involved in the piRNA-based transposon silencing system. Therefore, L1 is repressed at the post-transcriptional level in fetal male germ cells (prospermatogonia), and Maelstrom and HSP90α are likely involved in it. On the other hand, the piRNA-guided DNA methylation at the L1 promoter is important for transcriptional silencing in later (postnatal) stages, as evidenced by an increase in L1 mRNA after birth in the *Mili* and *Miwi2* mutants (23,42–43). HSP90α is possibly involved in several distinct steps in normal male germ cell development, because HSP90 is a chaperone that stabilizes a numerous client proteins in cytosol and in nucleus. Further study is needed to elucidate whether the deficiency in post-transcriptional regulation of retrotransposons in the *Hsp90α* KO fetal germ cells is directly linked to the deficiency in piRNA biogenesis.

Involvement of the HSP90 chaperone complexes in the mouse piRNA biogenesis was first suggested in the study of FKBP6, HSP90's co-chaperone, in which the authors showed that the *Fkbp6* KO mice had a defect in piRNA production, especially in MIWI2-bound piRNA (15). They also analyzed the effect of an HSP90 inhibitor, Geldanamycin (GA), on the piRNA biogenesis in cultured silkworm cells. The GA-treatment resulted in the accumulation of additional ~16-bp small RNA species which are likely byproducts of the RNA cleavage reaction by Ago3, a PIWI protein. Thus, they suggested that FKBP6 in mice and HSP90 in silkworm are involved in efficient recycling of the slicer enzyme. On the other hand, our computational analysis on the published sequence data revealed that the ping-pong byproducts are not accumulated in *Fkbp6* KO testes, similarly to the *HSP90α* KO testes. It is of note that, in *Hsp90α* KO testes, not only MIWI2-bound piRNAs but also MILI-bound piRNAs are reduced, indicating the presence of both FKBP6-dependent and FKBP6-independent actions of HSP90α. This seems to parallel with the insect piRNA system where at least two different HSP90 co-chaperones, Hop and Shutdown (Fkbp6 ortholog), are

required (12,14). The reduction of both MILI- and MIWI2-bound piRNAs by the *Hsp90α* mutation also suggests that the steps where HSP90α is involved in the piRNA biogenesis pathway include a step(s) upstream of the enzymatic reactions by MILI. Therefore, in analogy to the role of the insect HSP90 machinery in the formation of piRNA–PIWI complex (13) and siRNA–Ago2 complex (8), it is conceivable that the mouse HSP90α machinery has important roles in the formation and/or stability of the MILI–piRNA and MIWI2–piRNA complexes, the later being dependent on the FKBP6 co-chaperone.

The two cytosolic HSP90 isoforms were generated by gene duplication in the common ancestor of vertebrates and maintained thereafter, with the amino acid sequence and the expression pattern being diverged (44). However, whether the two isoforms are *functionally* diverged, particularly whether HSP90α with more tissue-specific expression has indispensable functions, remains controversial. A function specific to HSP90α would be its extracellular role in regulating matrix metalloproteinase activity and cancer metastasis (45). However, little is known about the difference in their intracellular functions. We previously demonstrated that HSP90α plays a more important role than HSP90β in the membrane translocation and presentation of exogenous antigens in mouse dendritic cells (16,24). In this study, our data revealed that HSP90α plays specific roles in the epigenetic regulatory systems against transposons during germ cell development. The single insect gene of HSP90 is also involved in piRNA biogenesis and transposon silencing (11,12), hinting that the function of the HSP90 machinery in piRNA biogenesis is conserved in metazoans. After gene duplication and functional divergence, this piRNA-related function may have become specific to *Hsp90α* in vertebrates or at least in mammals. Then, under the selection, *Hsp90α* may have become highly expressed in male germ cells.

ACCESSION NUMBERS

The small RNA sequencing data were deposited in GEO under the accession no. GSE54515.

SUPPLEMENTARY DATA

Supplementary Data are available at NAR Online.

ACKNOWLEDGEMENT

We thank Dr Alex Bortvin (Carnegie Institute) for supplying the anti-L1 antibody and Drs Takehisa Sakaguchi and Takashi Sado (Kyushu University) for technical advice. Ms Megumi Iwata is acknowledged for her technical assistance. We also thank Dr Akihiro Matsukawa and Mr Haruyuki Watanabe (Okayama University) for the use of the cryostat.

FUNDING

Grants-in-aid for Scientific Research from the Ministry of Education, Culture, Sports, Science, and Technology of Japan [22501027 to H.U., 20062010 to H.S., 25503003 and 21200037 to K.I.]; Takeda Foundation (to K.I. and H.U.); Naito Foundation (to H.U.); Women Researchers' Hand-in-Hand Program at Kyushu University (to T.I.). Funding for open access charge: The Takeda Foundation (to H.U.).
Conflict of interest statement. None declared.

REFERENCES

1. Taipale,M., Jarosz,D.F. and Lindquist,S. (2010). HSP90 at the hub of protein homeostasis: emerging mechanistic insights. *Nat. Rev. Mol. Cell Biol.*, **11**, 515–528.
2. Wandinger,S.K., Richter,K. and Buchner,J. (2008). The Hsp90 chaperone machinery. *J. Biol. Chem.*, **283**, 18473–18477.
3. Ohsako,S., Bunick,D. and Hayashi,Y. (1995). Immunocytochemical observation of the 90 KD heat shock protein (HSP90): high expression in primordial and pre-meiotic germ cells of male and female rat gonads. *J. Histochem. Cytochem.*, **43**, 67–76.
4. Lee,S.J. (1990). Expression of HSP86 in male germ cells. *Mol. Cell. Biol.*, **10**, 3239–3242.
5. Vanmuylder,N., Werry-Huet,A., Rooze,M. and Louryan,S. (2002). Heat shock protein HSP86 expression during mouse embryo development, especially in the germ-line. *Anat. Embryol.*, **205**, 301–306.
6. Iki,T., Yoshikawa,M., Nishikiori,M., Jaudal,M.C., Matsumoto-Yokoyama,E., Mitsuhara,I., Meshi,T. and Ishikawa,M. (2010). In vitro assembly of plant RNA-induced silencing complexes facilitated by molecular chaperone HSP90. *Mol. Cell*, **39**, 282–291.
7. Iwasaki,S., Kobayashi,M., Yoda,M., Sakaguchi,Y., Katsuma,S., Suzuki,T. and Tomari,Y. (2010). Hsc70/Hsp90 chaperone machinery mediates ATP-dependent RISC loading of small RNA duplexes. *Mol. Cell*, **39**, 292–299.
8. Miyoshi,T., Takeuchi,A., Siomi,H. and Siomi,M.C. (2010). A direct role for Hsp90 in pre-RISC formation in Drosophila. *Nat. Struc. Mol. Biol.*, **17**, 1024–1026.
9. Pare,J.M., Tahbaz,N., Lopez-Orozco,J., LaPointe,P., Lasko,P. and Hobman,T.C. (2009). Hsp90 regulates the function of argonaute 2 and its recruitment to stress granules and P-bodies. *Mol. Biol. Cell*, **20**, 3273–3284.
10. Pillai,R.S. and Chuma,S. (2012). piRNAs and their involvement in male germline development in mice. *Dev. Growth Differ.*, **54**, 78–92.
11. Specchia,V., Piacentini,L., Tritto,P., Fanti,L., D'Alessandro,R., Palumbo,G., Pimpinelli,S. and Bozzetti,M.P. (2010). Hsp90 prevents phenotypic variation by suppressing the mutagenic activity of transposons. *Nature*, **463**, 662–665.
12. Gangaraju,V.K., Yin,H., Weiner,M.M., Wang,J., Huang,X.A. and Lin,H. (2011). Drosophila Piwi functions in Hsp90-mediated suppression of phenotypic variation. *Nat. Genet.*, **43**, 153–158.
13. Izumi,N., Kawaoka,S., Yasuhara,S., Suzuki,Y., Sugano,S., Katsuma,S. and Tomari,Y. (2013). Hsp90 facilitates accurate loading of precursor piRNAs into PIWI proteins. *RNA*, **19**, 896–901.
14. Olivieri,D., Senti,K.A., Subramanian,S., Sachidanandam,R. and Brennecke,J. (2012). The cochaperone shutdown defines a group of biogenesis factors essential for all piRNA populations in Drosophila. *Mol. Cell*, **47**, 954–969.
15. Xiol,J., Cora,E., Koglgruber,R., Chuma,S., Subramanian,S., Hosokawa,M., Reuter,M., Yang,Z., Berninger,P., Palencia,A. *et al.* (2012). A role for Fkbp6 and the chaperone machinery in piRNA amplification and transposon silencing. *Mol. Cell*, **47**, 970–979.
16. Imai,T., Kato,Y., Kajiwara,C., Mizukami,S., Ishige,I., Ichiyanagi,T., Hikida,M., Wang,J.Y. and Udono,H. (2011). Heat shock protein 90 (HSP90) contributes to cytosolic translocation of extracellular antigen for cross-presentation by dendritic cells. *Proc. Natl. Acad. Sci. U.S.A.*, **108**, 16363–16368.
17. Kajiwara,C., Kondo,S., Uda,S., Dai,L., Ichiyanagi,T., Chiba,T., Ishido,S., Koji,T. and Udono,H. (2012). Spermatogenesis arrest caused by conditional deletion of Hsp90alpha in adult mice. *Biol. Open*, **1**, 977–982.
18. Watanabe,T., Chuma,S., Yamamoto,Y., Kuramochi-Miyagawa,S., Totoki,Y., Toyoda,A., Hoki,Y., Fujiyama,A., Shibata,T., Sado,T. *et al.* (2011). MITOPLD is a mitochondrial protein essential for nuage formation and piRNA biogenesis in the mouse germline. *Dev. Cell*, **20**, 364–375.

19. Martin,S.L. and Branciforte,D. (1993). Synchronous expression of LINE-1 RNA and protein in mouse embryonal carcinoma cells. *Mol. Cell. Biol.*, **13**, 5383–5392.
20. Kozomara,A. and Griffiths-Jones,S. (2014). miRBase: annotating high confidence microRNAs using deep sequencing data. *Nucleic Acids Res.*, **42**, D68–D73.
21. Jiang,H. and Wong,W.H. (2008). SeqMap: mapping massive amount of oligonucleotides to the genome. *Bioinformatics*, **24**, 2395–2396.
22. Jurka,J., Kapitonov,V.V., Pavlicek,A., Klonowski,P., Kohany,O. and Walichiewicz,J. (2005). Repbase Update, a database of eukaryotic repetitive elements. *Cytogen. Genome Res.*, **110**, 462–467.
23. Kuramochi-Miyagawa,S., Watanabe,T., Gotoh,K., Totoki,Y., Toyoda,A., Ikawa,M., Asada,N., Kojima,K., Yamaguchi,Y., Ijiri,T.W. *et al.* (2008). DNA methylation of retrotransposon genes is regulated by Piwi family members MILI and MIWI2 in murine fetal testes. *Genes Dev.*, **22**, 908–917.
24. Ichiyanagi,T., Imai,T., Kajiwara,C., Mizukami,S., Nakai,A., Nakayama,T. and Udono,H. (2010). Essential role of endogenous heat shock protein 90 of dendritic cells in antigen cross-presentation. *J. Immunol.*, **185**, 2693–2700.
25. Shoji,M., Tanaka,T., Hosokawa,M., Reuter,M., Stark,A., Kato,Y., Kondoh,G., Okawa,K., Chujo,T., Suzuki,T. *et al.* (2009). The TDRD9-MIWI2 complex is essential for piRNA-mediated retrotransposon silencing in the mouse male germline. *Dev. Cell*, **17**, 775–787.
26. Bastos,H., Lassalle,B., Chicheportiche,A., Riou,L., Testart,J., Allemand,I. and Fouchet,P. (2005). Flow cytometric characterization of viable meiotic and postmeiotic cells by Hoechst 33342 in mouse spermatogenesis. *Cytometry A*, **65**, 40–49.
27. Ichiyanagi,K., Li,Y., Watanabe,T., Ichiyanagi,T., Fukuda,K., Kitayama,J., Yamamoto,Y., Kuramochi-Miyagawa,S., Nakano,T., Yabuta,Y. *et al.* (2011). Locus- and domain-dependent control of DNA methylation at mouse B1 retrotransposons during male germ cell development. *Genome Res.*, **21**, 2058–2066.
28. Aravin,A.A., van der Heijden,G.W., Castaneda,J., Vagin,V.V., Hannon,G.J. and Bortvin,A. (2009). Cytoplasmic compartmentalization of the fetal piRNA pathway in mice. *PLoS Genet.*, **5**, e1000764.
29. Olovnikov,I., Aravin,A.A. and Fejes Toth,K. (2012). Small RNA in the nucleus: the RNA-chromatin ping-pong. *Curr. Opin. Genet. Dev.*, **22**, 164–171.
30. Wang,J., Saxe,J.P., Tanaka,T., Chuma,S. and Lin,H. (2009). Mili interacts with tudor domain-containing protein 1 in regulating spermatogenesis. *Curr. Biol.*, **19**, 640–644.
31. Chen,C., Nott,T.J., Jin,J. and Pawson,T. (2011). Deciphering arginine methylation: Tudor tells the tale. *Nat. Rev. Mol. Cell Biol.*, **12**, 629–642.
32. Vagin,V.V., Wohlschlegel,J., Qu,J., Jonsson,Z., Huang,X., Chuma,S., Girard,A., Sachidanandam,R., Hannon,G.J. and Aravin,A.A. (2009). Proteomic analysis of murine Piwi proteins reveals a role for arginine methylation in specifying interaction with Tudor family members. *Genes Dev.*, **23**, 1749–1762.
33. Saxe,J.P., Chen,M., Zhao,H. and Lin,H. (2013). Tdrkh is essential for spermatogenesis and participates in primary piRNA biogenesis in the germline. *EMBO J.*, **3**, 1869–1885.
34. Maloney,A., Clarke,P.A., Naaby-Hansen,S., Stein,R., Koopman,J.O., Akpan,A., Yang,A., Zvelebil,M., Cramer,R., Stimson,L. *et al.* (2007). Gene and protein expression profiling of human ovarian cancer cells treated with the heat shock protein 90 inhibitor 17-allylamino-17-demethoxygeldanamycin. *Cancer Res.*, **67**, 3239–3253.
35. Aravin,A.A., Sachidanandam,R., Bourc'his,D., Schaefer,C., Pezic,D., Toth,K.F., Bestor,T. and Hannon,G.J. (2008). A piRNA pathway primed by individual transposons is linked to de novo DNA methylation in mice. *Mol. Cell*, **31**, 785–799.
36. Soper,S.F., van der Heijden,G.W., Hardiman,T.C., Goodheart,M., Martin,S.L., de Boer,P. and Bortvin,A. (2008). Mouse maelstrom, a component of nuage, is essential for spermatogenesis and transposon repression in meiosis. *Dev. Cell*, **15**, 285–297.
37. Zheng,K., Xiol,J., Reuter,M., Eckardt,S., Leu,N.A., McLaughlin,K.J., Stark,A., Sachidanandam,R., Pillai,R.S. and Wang,P.J. (2010). Mouse MOV10L1 associates with Piwi proteins and is an essential component of the Piwi-interacting RNA (piRNA) pathway. *Proc. Natl. Acad. Sci. U.S.A.*, **107**, 11841–11846.
38. Oey,H.M., Youngson,N.A. and Whitelaw,E. (2011). The characterisation of piRNA-related 19mers in the mouse. *BMC Genomics*, **12**, 315.
39. Berninger,P., Jaskiewicz,L., Khorshid,M. and Zavolan,M. (2011). Conserved generation of short products at piRNA loci. *BMC Genomics*, **12**, 46.
40. Rutherford,S.L. and Lindquist,S. (1998). Hsp90 as a capacitor for morphological evolution. *Nature*, **396**, 336–342.
41. McLaren,A. (1999). Too late for the midwife toad: stress, variability and Hsp90. *Trends Genet.*, **15**, 169–171.
42. Carmell,M.A., Girard,A., de Kant,H.J., Bourc'his,D., Bestor,T.H., de Rooij,D.G. and Hannon,G.J. (2007). MIWI2 is essential for spermatogenesis and repression of transposons in the mouse male germline. *Dev. Cell*, **12**, 503–514.
43. Aravin,A.A., Sachidanandam,R., Girard,A., Fejes-Toth,K. and Hannon,G.J. (2007). Developmentally regulated piRNA clusters implicate MILI in transposon control. *Science*, **316**, 744–747.
44. Chen,B., Zhong,D. and Monteiro,A. (2006). Comparative genomics and evolution of the HSP90 family of genes across all kingdoms of organisms. *BMC Genomics*, **7**, 156.
45. Eustace,B.K., Sakurai,T., Stewart,J.K., Yimlamai,D., Unger,C., Zehetmeier,C., Lain,B., Torella,C., Henning,S.W., Beste,G. *et al.* (2004). Functional proteomic screens reveal an essential extracellular role for hsp90 alpha in cancer cell invasiveness. *Nat. Cell Biol.*, **6**, 507–514.

We have shown that transcriptional noise is well predicted by molecularly detailed models for the two most common promoter architectures in *E. coli* as the various genetic knobs are tuned. This agreement is not the result of fitting theory curves to data, because the predicted curves are generated using physical parameter values reported elsewhere in the literature and in that sense are zero-parameter predictions. Earlier reports of "bursty" transcription (*5*, *21*) are based on the observation that the Fano factor is greater than 1 for constitutive mRNA production (as well as direct kinetic measurements). Various explanatory hypotheses have been proposed, including transcriptional silencing via DNA condensation by nucleoid proteins (*22*), negative supercoiling induced by transcription, or the formation of long-lived "dead-end" initiation complexes (*23*). Although our data do not rule out these hypotheses, we find that extrinsic noise is sufficient to explain the deviation from Fano = 1 in our constitutive expression data (Fig. 2B). Thus, we find no need to invoke alternative hypotheses to explain the observed "burstiness" of constitutive transcription.

Many interesting earlier experiments make it difficult to interpret differences between promoters and induction conditions in terms of distinct physical parameters because of the wide variety of promoter architectures in play as well as the diverse mechanisms of induction. We have instead taken a "synthetic biology" approach of building promoters from the ground up. By directly controlling aspects of the promoter architecture, our goal has been to directly relate changes in promoter architecture to changes in observed gene expression variability. We believe that this work has demonstrated that mutations in regulatory DNA can alter gene expression noise. This suggests that gene expression noise may be a tunable property subject to evolutionary selection pressure, as mutations in regulatory DNA could provide greater fitness by increasing (or decreasing) variability. Demonstrating the relevance of this hypothesis in natural environments remains an ongoing challenge.

REFERENCES AND NOTES

1. J. Paulsson, M. Ehrenberg, *Phys. Rev. Lett.* **84**, 5447–5450 (2000).
2. A. Sanchez, H. G. Garcia, D. Jones, R. Phillips, J. Kondev, *PLOS Comput. Biol.* **7**, e1001100 (2011).
3. Y. Taniguchi *et al.*, *Science* **329**, 533–538 (2010).
4. W. J. Blake *et al.*, *Mol. Cell* **24**, 853–865 (2006).
5. L. H. So *et al.*, *Nat. Genet.* **43**, 554–560 (2011).
6. H. Salman *et al.*, *Phys. Rev. Lett.* **108**, 238105 (2012).
7. H. Maamar, A. Raj, D. Dubnau, *Science* **317**, 526–529 (2007).
8. A. Eldar, M. B. Elowitz, *Nature* **467**, 167–173 (2010).
9. G. M. Süel, R. P. Kulkarni, J. Dworkin, J. Garcia-Ojalvo, M. B. Elowitz, *Science* **315**, 1716–1719 (2007).
10. M. Thattai, A. van Oudenaarden, *Genetics* **167**, 523–530 (2004).
11. E. Kussell, S. Leibler, *Science* **309**, 2075–2078 (2005).
12. H. Salgado *et al.*, *Nucleic Acids Res.* **41**, D203–D213 (2013).
13. L. Bintu *et al.*, *Curr. Opin. Genet. Dev.* **15**, 125–135 (2005).
14. T. Kuhlman, Z. Zhang, M. H. Saier Jr., T. Hwa, *Proc. Natl. Acad. Sci. U.S.A.* **104**, 6043–6048 (2007).
15. J. M. Vilar, S. Leibler, *J. Mol. Biol.* **331**, 981–989 (2003).
16. See supplementary materials on *Science* Online.
17. A. Sánchez, J. Kondev, *Proc. Natl. Acad. Sci. U.S.A.* **105**, 5081–5086 (2008).
18. P. S. Swain, M. B. Elowitz, E. D. Siggia, *Proc. Natl. Acad. Sci. U.S.A.* **99**, 12795–12800 (2002).
19. R. C. Brewster, D. L. Jones, R. Phillips, *PLOS Comput. Biol.* **8**, e1002811 (2012).
20. P. Hammar *et al.*, *Science* **336**, 1595–1598 (2012).
21. I. Golding, J. Paulsson, S. M. Zawilski, E. C. Cox, *Cell* **123**, 1025–1036 (2005).
22. A. Sanchez, S. Choubey, J. Kondev, *Annu. Rev. Biophys.* **42**, 469–491 (2013).
23. N. Mitarai, I. B. Dodd, M. T. Crooks, K. Sneppen, *PLOS Comput. Biol.* **4**, e1000109 (2008).

ACKNOWLEDGMENTS

We thank H. J. Lee, C. Wiggins, Y. Lin, X. Zhu, F. Weinert, M. Rydenfelt, R. Milo, H. Garcia, N. Belliveau, and J. Sheung for useful discussions. Supported by NIH grants DP1 OD000217 (Directors Pioneer Award), R01 GM085286, and 1 U54 CA143869 (Northwestern PSOC Center); La Fondation Pierre Gilles de Gennes (R.P.); and the Donna and Benjamin M. Rosen Center for Bioengineering at Caltech (D.L.J.). Raw microscopy image data are archived in the Phillips laboratory at Caltech and are available upon request.

SUPPLEMENTARY MATERIALS

www.sciencemag.org/content/346/6216/1533/suppl/DC1
Materials and Methods
Supplementary Text
Figs. S1 to S11
Tables S1 to S3
References (*24–32*)

28 April 2014; accepted 4 November 2014
10.1126/science.1255301

IMMUNE TOLERANCE

Detection of self-reactive CD8$^+$ T cells with an anergic phenotype in healthy individuals

Yuka Maeda,[1] Hiroyoshi Nishikawa,[1]* Daisuke Sugiyama,[1] Danbee Ha,[1] Masahide Hamaguchi,[1] Takuro Saito,[1] Megumi Nishioka,[1,2] James B. Wing,[1] Dennis Adeegbe,[1] Ichiro Katayama,[2] Shimon Sakaguchi[1]*

Immunological tolerance to self requires naturally occurring regulatory T (T_{reg}) cells. Yet how they stably control autoimmune T cells remains obscure. Here, we show that T_{reg} cells can render self-reactive human CD8$^+$ T cells anergic (i.e., hypoproliferative and cytokine hypoproducing upon antigen restimulation) in vitro, likely by controlling the costimulatory function of antigen-presenting cells. Anergic T cells were naïve in phenotype, lower than activated T cells in T cell receptor affinity for cognate antigen, and expressed several coinhibitory molecules, including cytotoxic T lymphocyte–associated antigen-4 (CTLA-4). Using these criteria, we detected in healthy individuals anergic T cells reactive with a skin antigen targeted in the autoimmune disease vitiligo. Collectively, our results suggest that T_{reg} cell–mediated induction of anergy in autoimmune T cells is important for maintaining self-tolerance.

Naturally occurring CD25$^+$CD4$^+$ regulatory T (T_{reg}) cells, which specifically express the transcription factor FoxP3, actively maintain immunological self-tolerance and homeostasis (*1*). Developmental or functional anomalies of natural T_{reg} cells can cause autoimmune diseases (such as type I diabetes), allergy, and immunopathological diseases (such as inflammatory bowel disease) (*1*). How T_{reg} cells effectively control potentially hazardous self-reactive T cells in humans remains an open question. In particular, it is unknown whether T_{reg} cell–mediated suppression for a limited period has a critical long-lasting effect on cell fate and antigen reactivity of autoimmune T cells.

To address this issue, we examined proliferation, cytokine production, and cell fate of antigen-specific CD8$^+$ T cells in peripheral blood mononuclear cells (PBMCs) from healthy individuals stimulated in vitro with self-antigen peptide in the presence or absence of natural FoxP3$^+$CD25$^+$CD4$^+$ T_{reg} cells. Melan-A (also known as MART-1) used in the experiments is a self-antigen expressed by normal melanocytes and some melanoma cells and targeted in vitiligo vulgaris, an autoimmune disease of the skin (*2–5*). In the absence of T_{reg} cells, Melan-A–specific CD8$^+$ T cells [detectable by major histocompatibility complex (MHC) tetramers and peptide tetramers] expanded over 10 days from very few cells to a sizable fraction when cultured with peptide-pulsed autologous antigen-presenting cells (APCs) (Fig. 1A) (*6*). Natural T_{reg} cells, which appeared to be activated by endogenous self-peptides and class II MHC on autologous APCs (*7–9*), suppressed the expansion of Melan-A tetramer–positive (Tet$^+$) CD8$^+$ T cells in a dose-dependent manner. Similar stimulation with irrelevant peptide NY-ESO-1, another self- and tumor antigen, failed to induce Melan-ATet$^+$CD8$^+$ T cells. In cultures containing T_{reg} cells,

[1]Experimental Immunology, Immunology Frontier Research Center (IFReC-WPI), Osaka University, Osaka 565-0871, Japan. [2]Department of Dermatology, Graduate School of Medicine, Osaka University, Osaka 565-0871, Japan.
*Corresponding author. E-mail: shimon@ifrec.osaka-u.ac.jp (S.S.); nisihiro@ifrec.osaka-u.ac.jp (H.N.)

we noted an accumulation of Tet$^+$CD8$^+$ T cells that had divided once and then stopped further proliferation. This proliferation-aborted population increased in ratio, whereas the population under multiple cell divisions reciprocally decreased, in proportion to the number of added T_{reg} cells. The proliferation-aborted cells had significantly lower tetramer staining intensity than the cells that had vigorously proliferated in the absence of T_{reg} cells (peak a versus b in Fig. 1A, Fig. 1B, and fig. S1). The staining intensity of T cell receptor–αβ (TCR-αβ) chains was equivalent in both populations, which indicated that the lower tetramer staining intensity was not due to down-modulation of TCR but to lower TCR affinity for the Melan-A peptide, as supported by significantly lower ratios of tetramer versus TCR-αβ staining intensities (Fig. 1C). Functionally, they produced reduced levels of cytokines such as interferon-γ (IFN-γ), tumor necrosis factor-α (TNF-α), and interleukin 2 (IL-2) (Fig. 1, D and E), despite the addition of exogenous IL-2 to maintain cultured T cells. Furthermore, upon secondary stimulation, they remained hypoproliferative and produced very low amounts of cytokines (fig. S2). Thus, antigenic stimulation under T_{reg} cell–mediated suppression allows responder T cells with relatively low affinity TCRs for a self-antigen to divide once but prevents their further proliferation, which drives them into a profoundly and stably hypoproliferative and cytokine-hypoproducing state, which can be immunologically defined as "anergy" (*10–13*).

In contrast with anti–Melan-A responses, CD8$^+$ T cells from the same donor, who had detectable serum anticytomegalovirus (CMV) immunoglobulin G (IgG) antibody, had CMV peptide–specific T cells with a memory phenotype (fig. S3, A to D). CMV-specific CD8$^+$ T cells, whether they were in a naïve or memory cell fraction, vigorously proliferated and produced inflammatory cytokines even at a high T_{reg}-to-responder T cell ratio, with no significant differences in CMV tetramer staining intensity among CD8$^+$ T cells proliferating in the presence or absence of T_{reg} cells (fig. S3, E to H). However, high numbers of T_{reg} cells completely inhibited the proliferation of polyclonally activated naïve CD8$^+$ T cells without allowing a single cell division (fig. S4). The nondividing CD8$^+$ T cells proliferated as actively as nonsuppressed cells upon restimulation after removal of T_{reg} cells.

Collectively, T_{reg}-cell dosage, the immunological states of responder T cells (e.g., in a naïve or memory state), and their TCR affinity for cognate antigen contribute to T_{reg} cell–mediated induction of anergy. This is an active process and differs from a mere naïve nonproliferative state.

Microarray gene expression analysis revealed that activated or anergic Tet$^+$CD8$^+$ T cells or Tet$^-$CD8$^+$ T cells obtained from T_{reg}-absent or -present cell cultures were substantially different in gene expression profiles (Fig. 2A). As the most striking differences, the transcription of *CTLA4*, encoding the coinhibitory molecule CTLA-4 (*14*), was significantly up-regulated, whereas *BCL2*, encoding the apoptosis-inhibiting molecule B cell lymphoma-2 (BCL-2) (*15*), was down-regulated in anergic CD8$^+$ T cells, as confirmed by quantitative reverse transcription polymerase chain reaction (RT-PCR) (Fig. 2B). There were no significant differences in the expression of *PDCD1* encoding the coinhibitory molecule PD-1; the genes encoding the anergy-related molecules GRAIL, CBL-B, and EGR-2 (*16–19*); BAT3, TBX21, and EOMES, putative markers for exhausted CD8$^+$ T cells (*20*, *21*); and p27KIP1, a cyclin-dependent kinase inhibitor. Anergic CD8$^+$ T cells did not express FoxP3 (Fig. 2B and fig. S5A). The majority (>90%) of anergic CD8$^+$ T cells expressed both CTLA-4 and the chemokine receptor CCR7, which differed from the phenotype of activated or naïve CD8$^+$ T cells (Fig. 2, C and D, and fig. S5, B to D) (*22*, *23*). Functionally, during secondary stimulation of anergic Tet$^+$CD8$^+$ T cells with Melan-A peptide–pulsed APCs after removal of T_{reg} cells, antibody blockade of CTLA-4 and PD-1 at doses enhancing cytokine production by activated conventional T cells failed to rescue proliferation resistance or cytokine hypoproduction of anergic CD8$^+$ T cells (fig. S5E) (*24*). Addition of a high dose of IL-2 induced apoptosis in restimulated Tet$^+$CD8$^+$ T cells rather than abrogating their hyporesponsiveness. Nevertheless, anergic CD8$^+$ T cells were not in the process of immediate apoptosis (fig. S6), despite their lower *BCL2* expression than activated T cells (Fig. 2B). Thus, anergic CD8$^+$ T cells induced by T_{reg} cell–mediated suppression are distinct from activated or naïve T cells in gene and protein expression profiles. They also appear to be different from "exhausted" CD8$^+$ T cells, which develop as PD-1$^+$ hypoproliferative and cytokine-hypoproducing cells

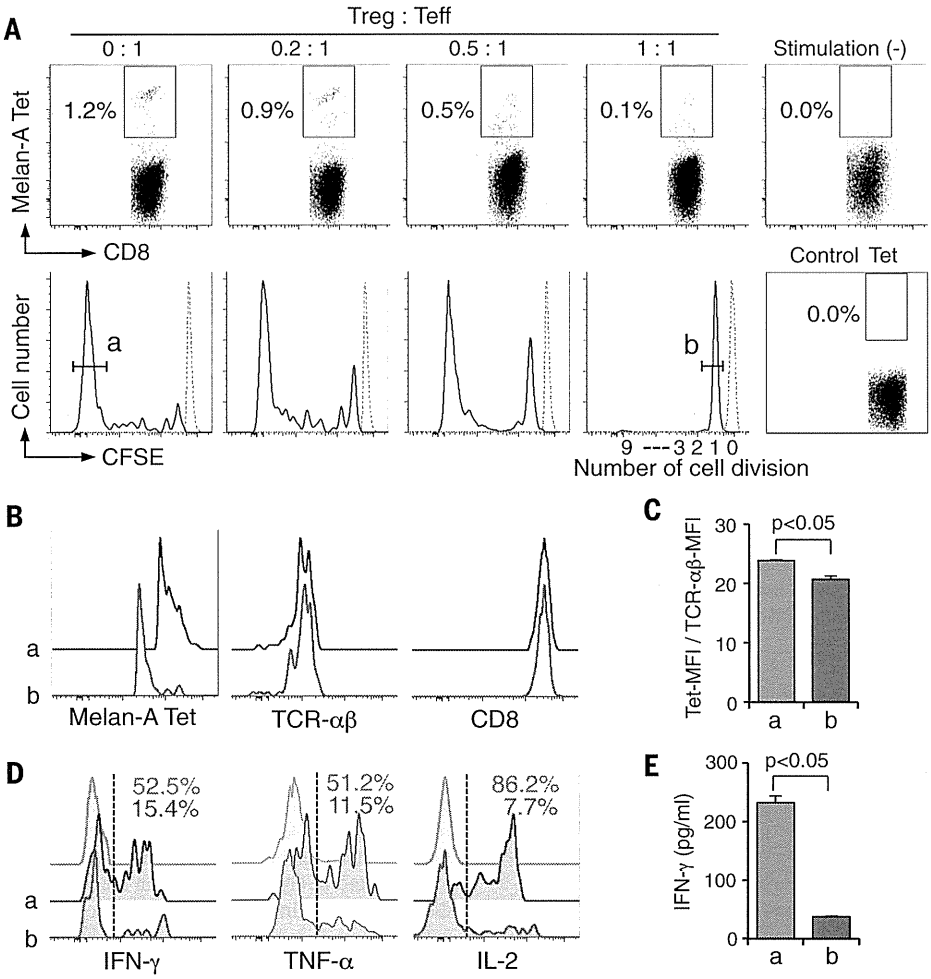

Fig. 1. Natural T_{reg} cells render low-affinity self-reactive CD8$^+$ T cells anergic upon antigen stimulation. (**A**) Melan-A–specific CD8$^+$ T cell induction. CFSE-labeled CD8$^+$ T cells of HLA-A*0201$^+$ healthy individuals were stimulated by T cell–depleted, γ-irradiated, and Melan-A_{26-35} peptide–pulsed APCs with graded numbers of CD25^{high}CD4$^+$ T_{reg} cells for 10 days (6). Dotted lines mean Tet$^-$CD8$^+$ cells showing no CFSE dilution. Control tet: NY-ESO-$1_{157-165}$/HLA-A*0201 tetramer. T_{eff} refers to CD8$^+$ effector T cells. (**B**) Tet, TCR-αβ, and CD8 staining of Tet$^+$CD8$^+$ T cells. Results in (A) and (B) are representative of 10 independent experiments. (**C**) Relative tetramer staining intensities, calculated as mean fluorescence intensity (MFI) of Tet/MFI of TCR-αβ staining of Tet$^+$CD8$^+$ T cells (n = 5). (**D** and **E**) Cytokine production of Tet$^+$CD8$^+$ T cells by intracellular staining (D) and enzyme-linked immunosorbent assay (E) (6). Representative result of three independent experiments. The labels a and b in (B) to (E) mean the cell accumulations like a or b in (A). Error bars indicate means ± SEM. The significance was assessed by Student's two-tailed paired t test.

in chronic viral infections and in tumor tissues, because exhausted $CD8^+$ T cells are reportedly $CCR7^-$, $CD45RA^-$, and $BAT3^+$, and their exhaustion can be rescued by a PD-1–blocking antibody (*21*, *24*–*26*).

T_{reg} cells suppress the activation and/or proliferation of responder T cells (*27*), at least in part, by down-regulating the expression of the costimulatory molecules CD80 and CD86 on APCs (fig. S7A) (*28*, *29*). To determine whether low expression or down-modulation of CD80 and CD86 on dendritic cells (DCs) was responsible for the induction of antigen-specific anergic $CD8^+$ T cells, we stimulated carboxyfluorescein succinimidyl ester (CFSE)–labeled $CD8^+$ T cells with autologous immature or mature DCs pulsed with Melan-A peptide in the presence of graded amounts of CTLA-4–immunoglobulin (CTLA-4Ig), which blocked CD80 and CD86 (fig. S7B) (*30*). In contrast to the vigorous proliferation of Tet^+CD8^+ T cells cultured with mature DCs, the majority of Tet^+CD8^+ T cells generated with immature DCs, and some with mature DCs with a high dose (100 μg/ml) of CTLA-4Ig, were proliferation-aborted after one cell division (Fig. 3A). The proliferation-aborted T cells (peaks c and d in Fig. 3A) were lower than proliferating T cells in Melan-A tetramer staining intensity (Fig. 3B), and highly expressed CTLA-4 and CCR7 (fig. S7, C and D); they formed a discrete CTLA-4/CCR7 double-positive population (Fig. 3C and fig. S7E). They produced significantly lower amounts of IFN-γ, TNF-α, and IL-2 compared with Tet^+CD8^+ cells, having proliferated in culture with mature DCs (fig. S7F). Similar to peptide stimulation, polyclonal antibody against CD3-specific monoclonal antibody (mAb) stimulation of $CTLA4^-$ naïve $CD8^+$ T cells in the presence of CTLA-4Ig produced cells that were proliferation-aborted after one cell division (fig. S8A). Notably, increasing CTLA-4Ig dose proportionally intensified CTLA-4 expression by the aborted cells, while stably maintaining their high CCR7 expression (fig. S8, A and B). Taken together, antigen presentation with low CD80 and CD86 costimulation is able to drive $CD8^+$ T cells to differentiate into $CTLA\text{-}4^+CCR7^+$ anergic cells. DCs with moderate CD80 and CD86 reduction can concurrently generate both

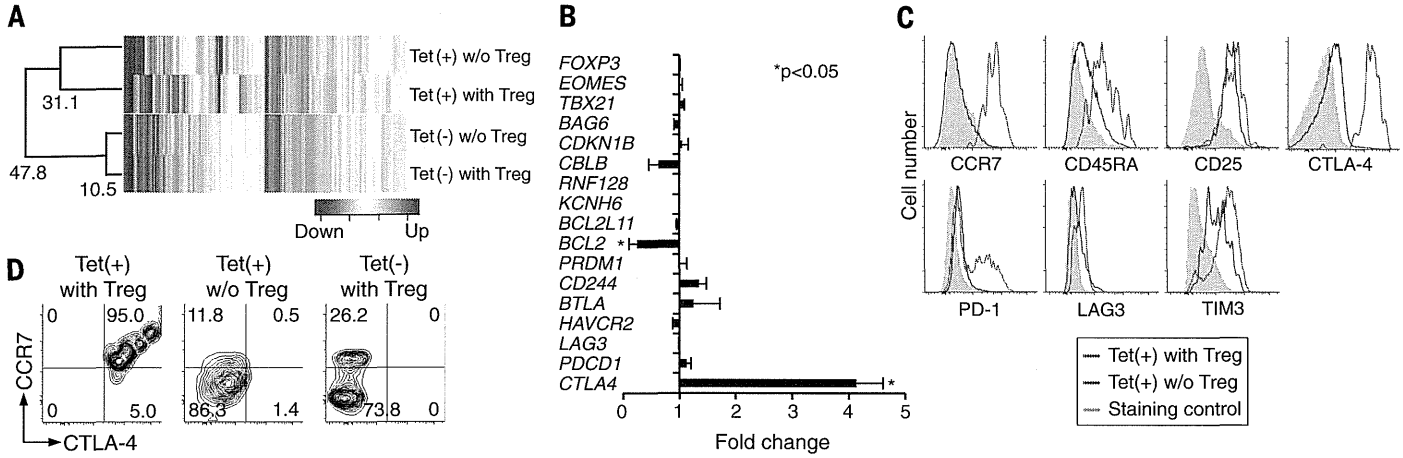

Fig. 2. Distinct phenotype and function of anergic $CD8^+$ T cells produced by T_{reg} cell suppression. (**A**) Global mRNA expression profile. Tet^+CD8^+ T cells induced at $CD8^+$ T cells: T_{reg} cell ratios of 1:0.5 and 1:0 were subjected to microarray analyses. Gene expression reportedly associated with $CD8^+$ T cell function was compared among the indicated four groups and expressed as a heat map. Correlation distances shown were calculated by h-clust (*6*). Representative of two independent experiments. (**B**) mRNA expression measured by quantitative real-time PCR. Fold changes of mRNA level as [Tet(+) with T_{reg}] versus [Tet(+) without T_{reg}] in five independent experiments are shown. Error bars indicate means ± SEM. (**C** and **D**) Expression of cell surface molecules by Tet^+CD8^+ T cells induced at $CD8^+$ T cells: T_{reg} cell ratios, 1:1 and 1:0. Representative histogram staining pattern (C) and contour plot staining pattern of CTLA-4 and CCR7 (D). Data are representative of five independent experiments (n = 10). The significance was assessed by Student's two-tailed paired t test.

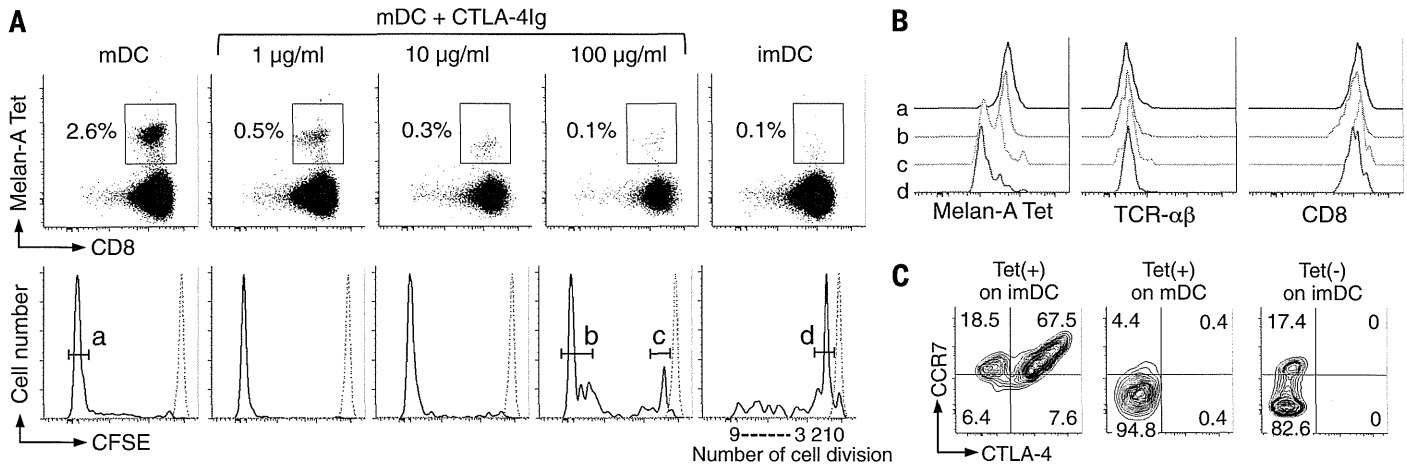

Fig. 3. DC expression of CD80 and CD86 controls the generation of $CTLA\text{-}4^+CCR7^+$ low-affinity anergic self-reactive T cells. (**A**) Melan-A–specific $CD8^+$ T cell induction. CFSE-labeled $CD8^+$ T cells of $HLA\text{-}A^*0201^+$ healthy individuals were stimulated with γ-irradiated, Melan-$A_{26\text{-}35}$ peptide–pulsed monocyte-derived immature or mature DCs. CTLA-4Ig was added into mature DCs cultures at indicated concentrations (*6*). (**B**) Tet, TCR-αβ, and CD8 staining intensity of Tet^+CD8^+ T cells shown in (A). (**C**) Representative contour plot staining pattern of Tet^+ or Tet^-CD8^+ T cells shown in (A) for CTLA-4 and CCR7. Data in (A) to (C) are representative of five independent experiments.

activated T cells and anergic T cells, in part, depending on TCR affinity.

The above in vitro findings prompted us to ask whether healthy individuals harbored such anergic self-reactive $CD8^+$ T cells. Direct ex vivo staining of $CD8^+$ T cells in PBMCs of healthy donors (n = 10) for Melan-A peptide and MHC tetramer, with $CD8^+$ T cells from vitiligo patients (n = 10) as a positive control, revealed that a small number of Tet^+CD8^+ T cells were indeed present in healthy individuals and constituted ~0.03% of $CD8^+$ T cells in PBMCs, which contrasted with high percentages (~0.1%) in vitiligo patients (Fig. 4, A and B) (*6*). Two-thirds of the former had a naïve ($CCR7^+CD45RA^+$) phenotype, whereas the majority of the latter had an effector or memory phenotype (Fig. 4C and fig. S9A) (*4*, *5*). The Tet^+CD8^+ T cells from healthy individuals had significantly lower tetramer staining intensity than those from vitiligo patients (Fig. 4, D and E). They expressed CTLA-4 at higher levels than Tet^+CD8^+ T cells from vitiligo patients or Tet^-CD8^+ T cells from healthy individuals, or activated $CD8^+$ T or natural T_{reg} cells (Fig. 4F and fig. S9, B to D), and ~90% of the $Tet^+CD45RA^+CD8^+$ cells were double positive for CTLA-4 and CCR7 (Fig. 4G and fig. S9B). Functionally, Tet^+CD8^+ T cells directly prepared from healthy donors scarcely produced IFN-γ, TNF-α, or IL-2, contrasting with active cytokine production by naïve Tet^-CD8^+ T cells (Fig. 4H) or Melan-A–specific $CD8^+$ T cells from vitiligo patients (*4*, *31*).

To determine further the function of these anergic T cells, we cocultured $CTLA\text{-}4^+$ and $CTLA\text{-}4^-$ fractions of naïve ($CCR7^+CD45RA^+$) $CD8^+$ T cells from healthy individuals and assessed the proliferative activity of Tet^+CD8^+ T cells present in each fraction (Fig. 4I). The $CTLA\text{-}4^+$ fraction, which constituted less than 10% of naïve $CD8^+$ T cells in healthy donors, contained the majority (~95%) of Melan-A Tet^+CD8^+ T cells before stimulation (Fig. 4, I to K). These $CTLA\text{-}4^+Tet^+$ cells were

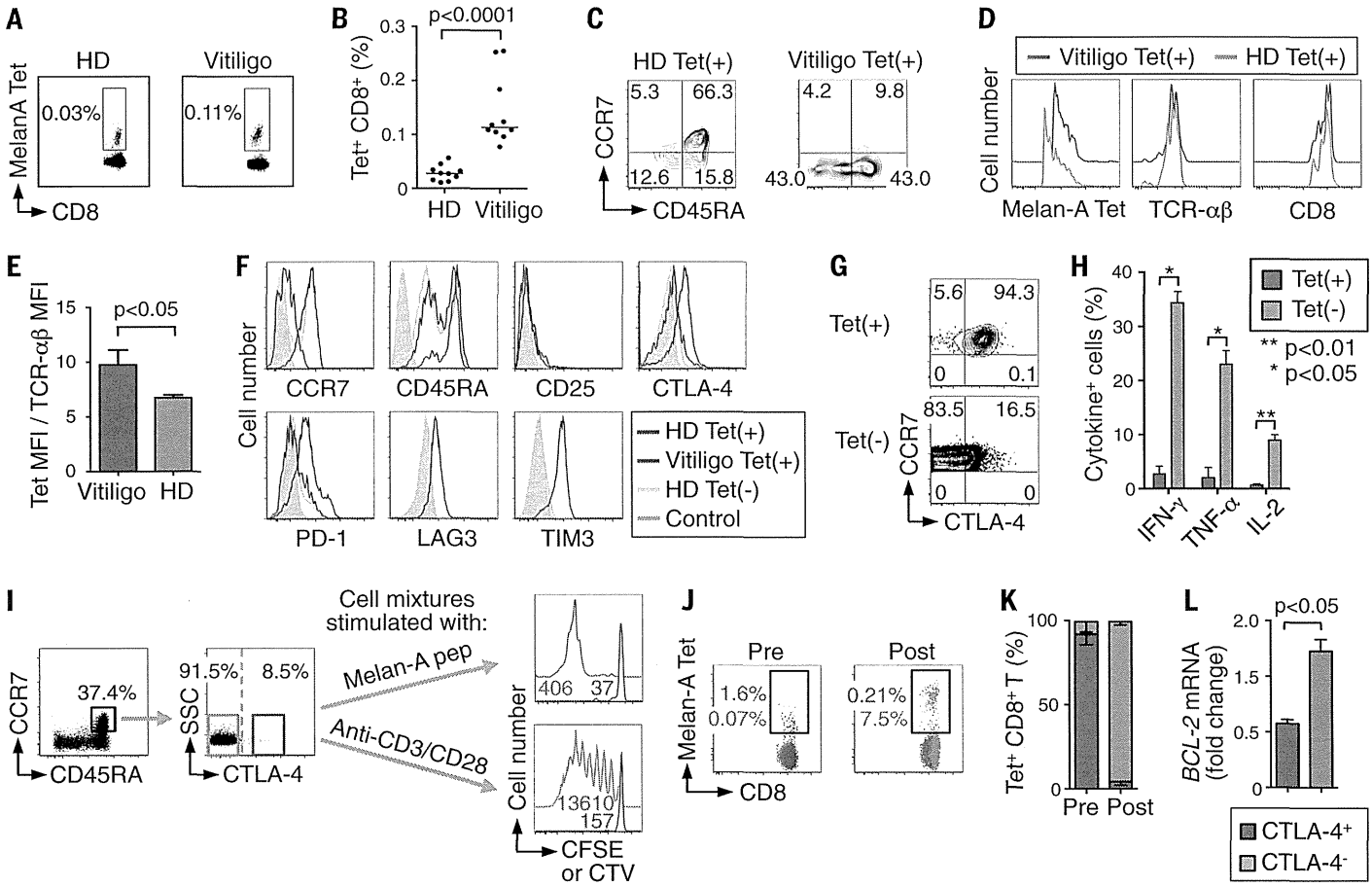

Fig. 4. Detection of low-affinity anergic self-reactive $CTLA\text{-}4^+CCR7^+CD8^+$ T cells in healthy individuals. (**A**) Melan-ATet^+CD8^+ T cells in PBMCs of a healthy donor (HD) and a vitiligo patient. (**B**) Percentages of Tet^+CD8^+ T cells in HDs and vitiligo patients (n = 10). (**C**) CCR7 and CD45RA expression by Tet^+CD8^+ T cells in an HD and a vitiligo patient. (**D**) Tet, TCR-αβ, and CD8 staining intensity of Tet^+CD8^+ T cells in an HD and a vitiligo patient. (**E**) Ratios of MFI of tetramer staining to MFI of TCR-αβ staining in Tet^+CD8^+ T cells in HDs and vitiligo patients (n = 4 each). (**F**) Expression of cell surface molecules by Tet^+ or Tet^-CD8^+ T cells in a representative HD and a vitiligo patient. (**G**) Representative staining for CTLA-4 and CCR7 of Tet^+ or Tet^- cells in $CD45RA^+CD8^+$ T cells of an HD. Data shown in (A), (C), (D), (F), and (G) are representative of four independent experiments. (**H**) Cytokine production by Tet^+CD8^+ T cells in HDs assessed by intracellular staining with $CCR7^+CD45RA^+Tet^-CD8^+$ T cells as control. Data summarize four independent experiments. (**I**) Proliferation and cytokine production of $CTLA\text{-}4^+$ or $CTLA\text{-}4^-$ naïve $CD8^+$ T cells in HDs. $CCR7^+CD45RA^+CD8^+$ T cells from HD PBMCs were further separated into $CTLA\text{-}4^+$ and $CTLA\text{-}4^-$ cells, labeled with Cell Trace Violet (CTV) or CFSE, respectively, mixed at a 1:1 ratio, stimulated with Melan-$A_{26\text{-}35}$ peptide–pulsed APCs for 10 days (top) or CD3/CD28-specific mAb for 5 days (bottom), and assessed for proliferation by CTV or CFSE dilution (red and blue, respectively) (*6*). Numbers in right two figures represent the numbers of cells in each cell fraction. SSC, side scatter. (**J**) Representative tetramer staining of the cell mixtures before (Pre) and after (Post) Melan-$A_{26\text{-}35}$ peptide stimulation for 10 days. Numbers represent percentages of Tet^+CD8^+ cells in the $CTLA\text{-}4^+$ or $CTLA\text{-}4^-$ fraction (red and blue, respectively). (**K**) Percentages of Tet^+CD8^+ T cells in the $CTLA\text{-}4^+$ (red) or $CTLA\text{-}4^-$ (blue) fraction in the cell mixtures before (Pre) and after (Post) cell culture as shown in (I) and (J). (**L**) *BCL2* mRNA expression of $CTLA\text{-}4^+CCR7^+CD45RA^+Tet^+CD8^+$ and $CTLA\text{-}4^-CCR7^+CD45RA^+Tet^+CD8^+$ T cells measured by quantitative real-time PCR. Data in (I) to (L) are representative of at least three independent experiments. Error bars indicate means ± SEM. The significance was assessed by Student's two-tailed paired t test.

hypoproliferative, low in *BCL2* expression, and prone to die upon Melan-A stimulation (Fig. 4, I to L). In contrast, the CTLA-4$^-$ fraction, which initially contained fewer than 5% of total Tet$^+$CD8$^+$ T cells, gave rise to proliferating Tet$^+$CD8$^+$ T cells, which made up ~95% of total Tet$^+$CD8$^+$ T cells after stimulation (Fig. 4, I to K). In addition, polyclonal stimulation of the cell mixtures with CD3-specific and CD28-specific mAb revealed that the CTLA-4$^+$ fraction as a whole was hypoproliferative (Fig. 4I) and cytokine hypoproducing (fig. S9E), in contrast with active proliferation and cytokine production of the CTLA-4$^-$ fraction.

These results collectively indicate that healthy individuals harbor at least two distinct populations of self-reactive CD8$^+$ T cells: one that is functionally anergic and expresses CTLA-4 and CCR7 and another that is CTLA-4$^-$ and naïve in function and phenotype. The latter, especially those with high-affinity TCRs, may become activated and expand upon self-antigen stimulation in the absence or reduction of natural T_{reg} cells, as shown in Fig. 1A.

Thus, anergic self-reactive T cells, which are phenotypically distinct from other T cells, are physiologically present in the immune system. They appear to be generated, at least in part, as a result of T_{reg}-mediated suppression, which can determine cell fate of responder T cells (i.e., activated, anergic, or ignorant) upon antigenic stimulation, depending on the number and suppressive activity of T_{reg} cells, the TCR affinity and differentiation states of responder T cells, and the condition of APCs. This T_{reg}-dependent switching of responder T cell fate can be a key target in controlling autoimmunity and tumor immunity, as illustrated by our analysis of Melan-A–specific immune responses, as well as a variety of other physiological and pathological immune responses.

REFERENCES AND NOTES

1. S. Sakaguchi, *Nat. Immunol.* **6**, 345–352 (2005).
2. P. G. Coulie *et al.*, *J. Exp. Med.* **180**, 35–42 (1994).
3. Y. Kawakami *et al.*, *Proc. Natl. Acad. Sci. U.S.A.* **91**, 6458–6462 (1994).
4. G. S. Ogg, P. Rod Dunbar, P. Romero, J. L. Chen, V. Cerundolo, *J. Exp. Med.* **188**, 1203–1208 (1998).
5. M. J. Pittet *et al.*, *J. Exp. Med.* **190**, 705–716 (1999).
6. Materials and methods are available as supplementary materials on *Science* Online.
7. M. Itoh *et al.*, *J. Immunol.* **162**, 5317–5326 (1999).
8. C. S. Hsieh, H. M. Lee, C. W. Lio, *Nat. Rev. Immunol.* **12**, 157–167 (2012).
9. T. Yamaguchi *et al.*, *Proc. Natl. Acad. Sci. U.S.A.* **110**, E2116–E2125 (2013).
10. M. K. Jenkins, R. H. Schwartz, *J. Exp. Med.* **165**, 302–319 (1987).
11. R. H. Schwartz, *Annu. Rev. Immunol.* **21**, 305–334 (2003).
12. F. Macián, S. H. Im, F. J. García-Cózar, A. Rao, *Curr. Opin. Immunol.* **16**, 209–216 (2004).
13. A. D. Wells, *J. Immunol.* **182**, 7331–7341 (2009).
14. A. H. Sharpe, G. J. Freeman, *Nat. Rev. Immunol.* **2**, 116–126 (2002).
15. P. E. Czabotar, G. Lessene, A. Strasser, J. M. Adams, *Nat. Rev. Mol. Cell Biol.* **15**, 49–63 (2014).
16. N. Anandasabapathy *et al.*, *Immunity* **18**, 535–547 (2003).
17. M. S. Jeon *et al.*, *Immunity* **21**, 167–177 (2004).
18. D. L. Mueller, *Nat. Immunol.* **5**, 883–890 (2004).
19. Y. Zheng, Y. Zha, G. Driessens, F. Locke, T. F. Gajewski, *J. Exp. Med.* **209**, 2157–2163 (2012).
20. M. A. Paley *et al.*, *Science* **338**, 1220–1225 (2012).
21. M. Rangachari *et al.*, *Nat. Med.* **18**, 1394–1400 (2012).
22. F. Sallusto, D. Lenig, R. Förster, M. Lipp, A. Lanzavecchia, *Nature* **401**, 708–712 (1999).
23. M. A. Williams, M. J. Bevan, *Annu. Rev. Immunol.* **25**, 171–192 (2007).
24. D. L. Barber *et al.*, *Nature* **439**, 682–687 (2006).
25. S. D. Blackburn *et al.*, *Nat. Immunol.* **10**, 29–37 (2009).
26. E. J. Wherry, *Nat. Immunol.* **12**, 492–499 (2011).
27. E. M. Shevach, *Immunity* **30**, 636–645 (2009).
28. K. Wing *et al.*, *Science* **322**, 271–275 (2008).
29. O. S. Qureshi *et al.*, *Science* **332**, 600–603 (2011).
30. J. A. Bluestone, E. W. St. Clair, L. A. Turka, *Immunity* **24**, 233–238 (2006).
31. K. S. Lang *et al.*, *J. Invest. Dermatol.* **116**, 891–897 (2001).

ACKNOWLEDGMENTS

We thank Y. Tada, K. Teshima, and Y. Funabiki for technical assistance. The data presented in this paper are tabulated in the main paper and in the supplementary materials. Microarray data are deposited in GSE63129. This study was supported by Grants-in-Aid for Specially Promoted Research (to S.S., no. 20002007) and for Scientific Research (i) (to S.S., no. 26253030) and (ii) (to H.N., no. 23300354 and 26290054) from the Ministry of Education, Culture, Sports, Science, and Technology of Japan; Core Research for Evolutional Science and Technology (CREST) from Japan Science and Technology Agency (to S.S.); Health and Labor Sciences Research Grants, Research on Applying Health Technology (H24-Clinical Cancer Research-general-006 to H.N.) from the Ministry of Health, Labor, and Welfare, Japan, the Cancer Research Institute CLIP grant to H.N. All authors have no competing financial interest.

SUPPLEMENTARY MATERIALS

www.sciencemag.org/content/346/6216/1536/suppl/DC1
Materials and Methods
Supplemental Text
Figs. S1 to S9
References (*32*–*37*)

21 October 2014; accepted 20 November 2014
10.1126/science.aaa1292

CellPress

Immunity
Article

Interleukin-10-Producing Plasmablasts Exert Regulatory Function in Autoimmune Inflammation

Masanori Matsumoto,[1,4] Akemi Baba,[1] Takafumi Yokota,[5] Hiroyoshi Nishikawa,[2] Yasuyuki Ohkawa,[7] Hisako Kayama,[3,6] Axel Kallies,[8,9] Stephen L. Nutt,[8,9] Shimon Sakaguchi,[2] Kiyoshi Takeda,[3,6] Tomohiro Kurosaki,[1,4,*] and Yoshihiro Baba[1,4,*]
[1]Laboratory for Lymphocyte Differentiation
[2]Laboratory for Experimental Immunology
[3]Laboratory for Immune Regulation
WPI Immunology Frontier Research Center, Osaka University, Suita, Osaka 565-0871, Japan
[4]Laboratory for Lymphocyte Differentiation, RIKEN Center for Integrative Medical Sciences (IMS), Yokohama, Kanagawa 230-0045, Japan
[5]Department of Hematology and Oncology
[6]Department of Microbiology and Immunology
Graduate School of Medicine, Osaka University, Suita, Osaka 565-0871, Japan
[7]Department of Advanced Medical Initiatives, JST-CREST, Faculty of Medicine, Kyushu University, Fukuoka 812-8582, Japan
[8]The Walter and Eliza Hall Institute of Medical Research, Parkville, VIC 3050, Australia
[9]Department of Medical Biology, The University of Melbourne, Parkville, VIC 3010, Australia
*Correspondence: kurosaki@ifrec.osaka-u.ac.jp (T.K.), babay@ifrec.osaka-u.ac.jp (Y.B.)
http://dx.doi.org/10.1016/j.immuni.2014.10.016

SUMMARY

B cells can suppress autoimmunity by secreting interleukin-10 (IL-10). Although subpopulations of splenic B lineage cells are reported to express IL-10 in vitro, the identity of IL-10-producing B cells with regulatory function in vivo remains unknown. By using IL-10 reporter mice, we found that plasmablasts in the draining lymph nodes (dLNs), but not splenic B lineage cells, predominantly expressed IL-10 during experimental autoimmune encephalomyelitis (EAE). These plasmablasts were generated only during EAE inflammation. Mice lacking plasmablasts by genetic ablation of the transcription factors Blimp1 or IRF4 in B lineage cells developed an exacerbated EAE. Furthermore, IRF4 positively regulated IL-10 production that can inhibit dendritic cell functions to generate pathogenic T cells. Our data demonstrate that plasmablasts in the dLNs serve as IL-10 producers to limit autoimmune inflammation and emphasize the importance of plasmablasts as IL-10-producing regulatory B cells.

INTRODUCTION

In the context of autoimmune disorders, B cells can be pathogenic effectors through their production of autoantibodies. However, evidence is accumulating that B cells can also be immunosuppressive in T-cell-mediated autoimmune and inflammatory diseases. Examples are collagen-induced arthritis (CIA) (Mauri et al., 2003), systemic lupus erythematosus (SLE) (Watanabe et al., 2010), and experimental autoimmune encephalomyelitis (EAE), an animal model of human multiple sclerosis (MS) (Fillatreau et al., 2002; Matsushita et al., 2008). The regulatory function of B cells is considered to be mainly determined by the secretion of interleukin-10 (IL-10), which is controlled by signals from Toll-like receptors (TLRs) (Lampropoulou et al., 2008), CD40 (Mauri et al., 2003), and B cell antigen receptors (BCR) (Fillatreau et al., 2002). To date, several unique populations of splenic IL-10-competent B cells (regulatory B cells) have been described. They include $CD21^{hi}CD23^{hi}IgM^{hi}$ transitional 2-marginal zone precursor (T2-MZP) B cells (Evans et al., 2007) and $CD1d^{hi}CD5^{+}$ B cells (Matsushita et al., 2008) that have been reported to inhibit autoimmunity. In addition, splenic $CD138^{+}$ plasma cells were also reported to express IL-10 (Shen et al., 2014). However, these populations produce detectable IL-10 only when stimulated ex vivo. Thus, despite progress made in understanding the importance of B-cell-derived IL-10, there has been no definitive identification of in vivo IL-10-producing B cells with regulatory function during autoimmunity.

In humans, a role for B-cell-derived IL-10 in downregulation of inflammatory reactions has been suggested in autoimmune diseases such as MS or SLE (Blair et al., 2010; Duddy et al., 2007; Mauri and Bosma, 2012). Treatment with rituximab for B cell depletion efficiently ameliorated the disease progression in some autoimmune diseases, presumably because of elimination of pathogenic B cells (Gürcan et al., 2009). However, this might work in part because of selective survival and repopulation of regulatory B cell subsets (Duddy et al., 2007; Todd et al., 2014). The functional and clinical importance of human IL-10-competent B cells has begun to be elucidated but more must be learned about their characteristics.

Here we have exploited IL-10 reporter mice to identify in vivo IL-10-producing B cells and demonstrate that $CD138^{+}$ plasmablasts, proliferating immature plasma cells, are the predominant source of IL-10 during EAE development. IL-10-producing plasmablasts were generated specifically in the draining lymph nodes (dLNs) but not in the spleen after EAE induction. By genetic

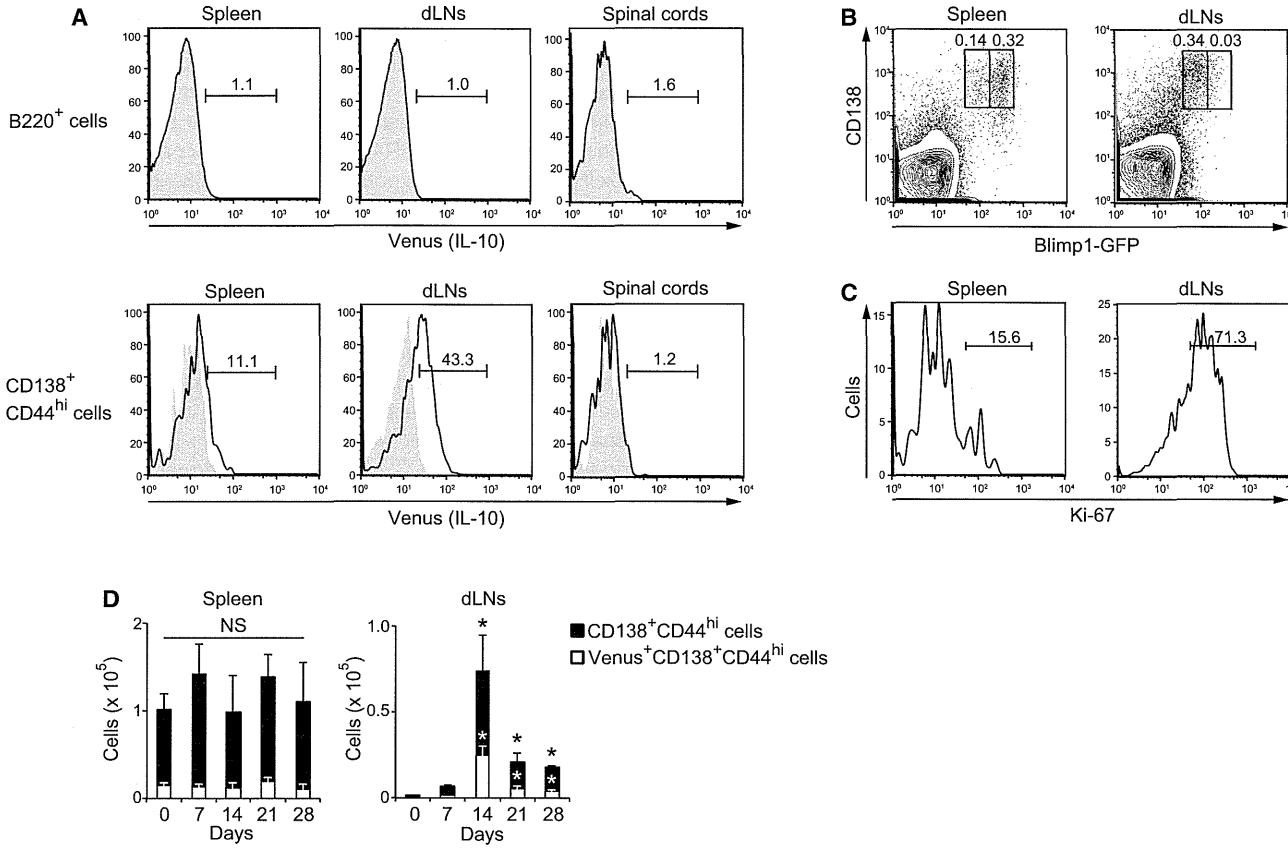

Figure 1. Plasmablasts Are the Dominant IL-10-Producing B Lineage Cells during EAE

(A) Flow cytometry of Venus expression in B220$^+$ and CD138$^+$CD44^{hi} cells harvested from spleen, dLNs, and spinal cords of wild-type (shaded histogram) and *Il10*$^{Venus/+}$ (open histogram) mice 14 days after MOG_{35-55} immunization. Percentages of Venus$^+$ B cells are shown.

(B) Flow cytometry of cells from spleen and dLNs of *Prdm1*$^{gfp/+}$ mice 14 days after MOG_{35-55} immunization. GFP^{int} and GFP^{hi} populations of CD138$^+$ cells are gated and their percentages are shown.

(C) Flow cytometry of CD138$^+$CD44^{hi} cells from spleen and dLNs of wild-type mice 14 days after MOG_{35-55} immunization. Percentages of Ki-67$^+$ cells are shown. Data are representative of at least three independent experiments in (A)–(C).

(D) Absolute number of CD138$^+$CD44^{hi} or their Venus$^+$ cells from spleen and dLNs of *Il10*$^{Venus/+}$ mice before and 7, 14, 21, and 28 days after MOG_{35-55} immunization. Data are representative of two independent experiments. Data are presented as mean ± SEM for four mice. NS, not significant. *$p < 0.05$ versus day 0 (Welch's t test).

See also Figure S1.

approaches, we show that plasmablasts in the dLNs were critical for limiting EAE progression. In addition, IL-10 production by plasmablasts requires IRF4 and can prevent dendritic cells from generating pathogenic T cells. Furthermore, human plasmablasts also preferentially secrete IL-10, further highlighting plasmablasts as the IL-10-producing regulatory B cells.

RESULTS

Plasmablasts Are the Main IL-10-Producing B Cells during EAE

To identify in vivo IL-10-producing B cells and their distribution during autoimmune disease, we elicited EAE in mice carrying a transgene of *Venus*, a variant of yellow fluorescent protein (*Il10*$^{Venus/+}$), which allows tracking of IL-10$^+$ cells (Atarashi et al., 2011). Although previous reports suggested that several splenic B cell subsets can produce IL-10 (Mauri and Bosma, 2012; Yanaba et al., 2008), we observed little Venus expression in B220$^+$ B cells before and 14 days after immunization with myelin oligodendrocyte glycoprotein peptide (MOG_{35-55}) (Figure 1A and Figures S1A–S1D available online). In contrast, CD138$^+$CD44^{hi} cells expressed Venus markedly in the dLNs, only modestly in spleen, and not at all in the spinal cords (Figures 1A, S1C, and S1D). ELISA assays also demonstrated that the CD138$^+$CD44^{hi} population expressing Venus had a potential to produce IL-10 (Figure S1E). CD138$^+$ cells are composed of highly proliferative plasmablasts and nondividing plasma cells that express intermediate and high amounts of Blimp1 (encoded by the *Prdm1*), respectively (Kallies et al., 2004). By utilizing EAE-induced heterozygous *Prdm1*^{gfp} knockin mice (*Prdm1*$^{gfp/+}$), we confirmed that CD138$^+$ cells in spleen and dLNs were largely GFP^{hi} plasma cells and GFP^{int} plasmablasts, respectively (Figure 1B). CD138$^+$CD44^{hi} cells in dLNs, but not spleen, were proliferating, as demonstrated by Ki-67 staining

(Figure 1C). Whereas the absolute number of CD138$^+$CD44^{hi} cells and their Venus$^+$ cells was essentially constant in spleen, those in dLNs expanded to a peak on day 14 after MOG_{35-55} immunization (Figure 1D). Thus, these results indicate that CD138$^+$ plasmablasts in dLNs are the principal IL-10-producing B lineage cells during EAE.

Plasmablasts in the dLNs Negatively Regulate EAE Inflammation

A key question is whether IL-10$^+$CD138$^+$ cells are functionally competent to inhibit EAE. To directly address this issue, we elicited EAE in mice conditionally lacking Blimp1 in B lineage cells by crossing of *Prdm1*$^{f/f}$ with *Mb1*$^{Cre/+}$ mice (called *Prdm1*$^{f/f}$*Mb1*$^{Cre/+}$ here). Plasma cell differentiation and antibody responses were impaired in these mice (Figures S2A and S2B). EAE development in *Prdm1*$^{f/f}$*Mb1*$^{Cre/+}$ mice was greatly exacerbated as compared to *Mb1*$^{Cre/+}$ control mice (Figure 2A). Consistent with the exacerbated EAE, CD4$^+$ T cells, particularly those producing interferon-γ (IFN-γ) (Th1 cells) and IL-17 (Th17 cells), increased in the spinal cords of *Prdm1*$^{f/f}$*Mb1*$^{Cre/+}$ mice (Figure 2B). When stimulated with MOG_{35-55}, *Prdm1*$^{f/f}$*Mb1*$^{Cre/+}$ LN cells produced more IFN-γ and IL-17 than *Mb1*$^{Cre/+}$ cells (Figure 2C). Thus, we conclude that CD138$^+$ plasmablasts/plasma cells limit EAE inflammation.

Given that IL-10-producing CD138$^+$ cells are detected in both spleen and dLNs during EAE, it remained important to test which secondary lymphoid organ is critical for EAE attenuation. L-selectin (CD62L), also known as Sell, is an essential homing receptor that governs migration into the peripheral LNs. To explore the involvement of LN B cells in EAE suppression, we generated mixed bone marrow (BM) chimeras by transferring a mixture of BM cells from μMT (80%) and *Sell*$^{-/-}$ (20%) mice into lethally irradiated wild-type mice. The Sell deficiency was restricted to B cells in the resultant BM chimera (B-*Sell*$^{-/-}$) mice. These mice lacked B lineage cells in LNs, but not spleen, and exhibited increased disease severity compared with control mice (Figure 2D). In striking contrast, mice that had splenectomy developed EAE normally (Figure 2E). B cell population and plasmablast differentiation in the dLNs was not affected by splenectomy. Collectively, these data suggest that plasmablasts in the dLNs negatively regulate EAE, but that splenic B lineage cells are dispensable for its suppression.

Nevertheless, published studies have claimed a functionally important role of splenic B cells to reduce EAE in adaptive transfer experiments (Fillatreau et al., 2002; Matsushita et al., 2008). Based on our above findings, we reasoned that adoptively transferred splenic B cells might give rise to plasmablasts in the dLNs that then regulate EAE. We therefore examined EAE in μMT mice with adoptively transferred splenic B cells isolated from *Prdm1*$^{f/f}$*Mb1*$^{Cre/+}$ or *Sell*$^{-/-}$ mice and control mice. Although the mice that received B cells from control mice resolved EAE symptoms, these suppressive effects were not observed when *Prdm1*$^{f/f}$*Mb1*$^{Cre/+}$ and *Sell*$^{-/-}$ B cells were transferred (Figures 2F and 2H). As expected, plasmablast differentiation from control B cells, but not *Prdm1*$^{f/f}$*Mb1*$^{Cre/+}$ and *Sell*$^{-/-}$ B cells, occurred in LNs (Figures 2G and 2I). These results suggest that splenic B cells can suppress EAE in an adoptive transfer setting but that their plasmablast differentiation in the dLNs might be required.

EAE Induces Generation of GC-Independent Plasmablasts that Produce IL-10 Preferentially

To gain insight into cellular aspects of IL-10-producing plasmablasts in the dLNs, we first investigated the cell surface phenotype. Most LN plasmablasts in EAE mice expressed high amounts of CD43, CXCR4, and major histocompatibility complex II (MHCII) and low amounts of B220, CD38, and CXCR5 (Figure 3A). Many of them also had undergone immunoglobulin (Ig) class-switch recombination (Figure 3B), which commonly occurs in both extrafollicular and germinal center (GC) responses (Klein and Dalla-Favera, 2008). Because an extensive expansion of GC B cells in the dLNs was detected during EAE (Figure 3C), we investigated the involvement of GCs in regulatory plasmablast generation. We elicited EAE in mice in which the transcription factor Bcl6 was functionally disrupted by inserting a YFP gene in both of the *Bcl6* alleles (*Bcl6*$^{yfp/yfp}$) (Kitano et al., 2011) and found that *Bcl6*$^{yfp/yfp}$ mice exhibited normal EAE despite of their lack of GC B cells (Figures 3D and 3E). The plasmablast generation was not significantly influenced by loss of Bcl6 (Figure 3E). Thus, EAE attenuation does not necessarily require GC responses.

We next assessed the potential contribution of anti-inflammatory cytokines besides IL-10 in plasmablasts. Because published studies have suggested that splenic B cells or plasma cells secrete IL-4, IL-13, IL-35, and transforming growth factor-β (TGF-β) (Mauri, 2010; Shen et al., 2014), we examined their expression in plasmablasts by quantitative RT-PCR analysis. In agreement with our data obtained with IL-10 reporter mice, CD138$^+$CD44^{hi} plasmablasts, but not CD19$^+$CD138$^-$ B cells, highly expressed IL-10 (Figure 3F). By contrast, the amount of *Il4*, *Il13*, *Il27* (*Il27b/p28*), *Il35* (*Il12a/Il27b*), and *Tgfb1* mRNA in CD138$^+$CD44^{hi} cells was decreased or comparable to that in CD19$^+$ cells. Consistent with that, ELISA and Bio-Plex suspension assay demonstrated preferential IL-10 secretion by CD138$^+$CD44^{hi} cells (Figure 3G). Although IL-6 and IFN-γ produced by B cells have been reported to contribute to EAE pathogenesis (Barr et al., 2012; Matsushita et al., 2006), CD138$^+$ CD44^{hi} cells had little expression of their mRNA and proteins. Collectively, EAE-induced plasmablasts in the dLNs predominantly produce IL-10.

IRF4 Is Essential for Plasmablast IL-10 Production

We next investigated the mechanisms by which plasmablasts produce IL-10. In a previous study, we found that B cells could secrete IL-10 after BCR stimulation in a Ca^{2+} influx-dependent way (Matsumoto et al., 2011). However, this occurred only when B cells were preactivated with TLR agonists. Thus, we reasoned that TLR-dependent transcription factors would be required for plasmablast differentiation and/or IL-10 production. To this end, LPS-stimulated B cells from *Prdm1*$^{gfp/+}$ mice were sorted on the basis of GFP and CD138 expression followed by stimulation with anti-IgM (Figure 4A). IL-10 secretion was restricted to GFP$^+$ fractions and drastically enhanced by BCR ligation (Figure 4B). Because both CD138$^+$GFP$^+$ and CD138$^-$GFP$^+$ populations are known to have characteristics of antibody secretion and proliferative responses (Kallies et al., 2004), we concluded that plasmablasts are the principal IL-10 producers in vitro. Unexpectedly, however, B cells lacking Blimp1 proteins secreted IL-10 normally despite having impaired CD138$^+$

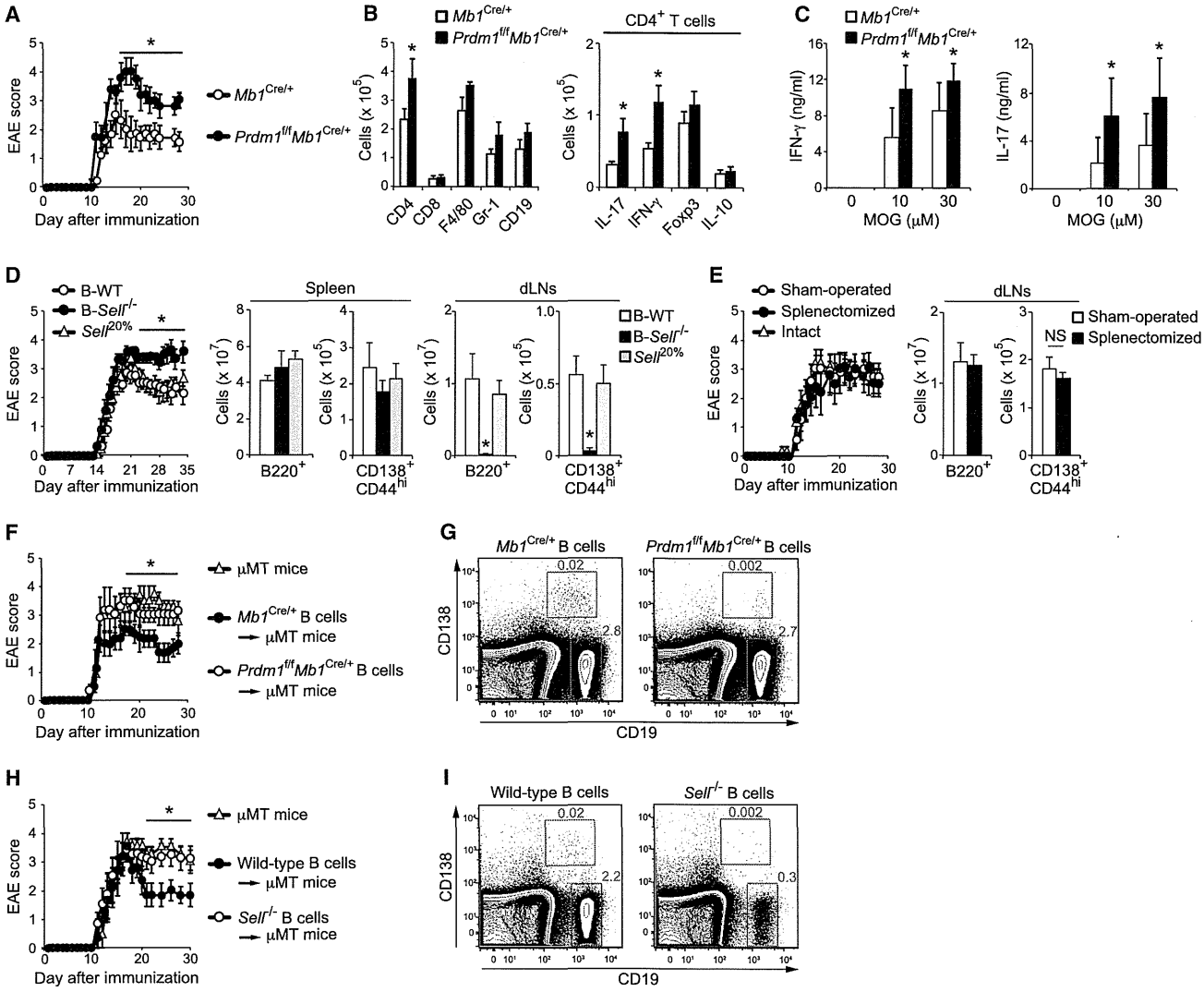

Figure 2. Plasmablasts in the dLNs Negatively Regulate EAE Inflammation

(A) Clinical EAE scores for *Mb1*$^{Cre/+}$ and *Prdm1*$^{f/f}$*Mb1*$^{Cre/+}$ mice immunized with MOG_{35-55}. The EAE score is shown as mean ± SEM for six to seven mice.

(B) Absolute number of cells from spinal cords harvested from *Mb1*$^{Cre/+}$ and *Prdm1*$^{f/f}$*Mb1*$^{Cre/+}$ mice 14 days after MOG_{35-55} immunization. Data are presented as mean ± SEM for five mice.

(C) ELISA of IFN-γ and IL-17 by cells isolated from the dLNs of *Mb1*$^{Cre/+}$ and *Prdm1*$^{f/f}$*Mb1*$^{Cre/+}$ mice 14 days after EAE induction followed by stimulation with MOG_{35-55} for 48 hr. Data are presented as mean ± SD.

(A–C) *p < 0.05 versus *Mb1*$^{Cre/+}$ mice (Mann-Whitney U test).

(D) Clinical EAE scores for B-*Sell*$^{-/-}$ (chimeric mice generated by transplanting a mixture of BM cells from μMT (80%) and *Sell*$^{-/-}$ (20%) mice and two control chimera groups: wild-type mice lethally irradiated and reconstituted with 80% μMT plus 20% wild-type bone marrow (B-WT) or reconstituted with 80% wild-type plus 20% *Sell*$^{-/-}$ bone marrow (*Sell*$^{20\%}$). The absolute number of B220$^+$ and CD138$^+$CD44^{hi} cells harvested from spleen and dLNs of chimeras 14 days after MOG_{35-55} immunization is shown on the right. Data are shown as mean ± SEM for five to ten mice. *p < 0.05 versus B-WT mice (Mann-Whitney U test).

(E) Clinical EAE scores for sham-operated, splenectomized, and intact wild-type mice immunized with MOG_{35-55}. Absolute number of B220$^+$ and CD138$^+$CD44^{hi} cells from dLNs of sham-operated and splenectomized mice 14 days after MOG_{35-55} immunization is shown on the right. Data are shown as mean ± SEM for five to seven mice. NS, not significant (Mann-Whitney U test).

(F) Clinical EAE scores for μMT mice immunized with MOG_{35-55} after injecting splenic B cells harvested from *Mb1*$^{Cre/+}$ and *Prdm1*$^{f/f}$*Mb1*$^{Cre/+}$ mice 28 days after EAE induction. The EAE score is shown as mean ± SEM for five to six mice. *p < 0.05 versus *Prdm1*$^{f/f}$*Mb1*$^{Cre/+}$ B cells (Mann-Whitney U test).

(G) Flow cytometry of cells from dLNs of μMT mice immunized for 12 days with MOG_{35-55} after injecting splenic *Mb1*$^{Cre/+}$ and *Prdm1*$^{f/f}$*Mb1*$^{Cre/+}$ B cells.

(H) Clinical EAE scores for μMT mice immunized with MOG_{35-55} after injecting splenic B cells harvested from wild-type and *Sell*$^{-/-}$ mice. The EAE score is shown as mean ± SEM for five to nine mice. *p < 0.05 versus *Sell*$^{-/-}$ B cells (Mann-Whitney U test).

(I) Flow cytometry of cells from dLNs of μMT mice immunized for 12 days with MOG_{35-55} after injecting splenic wild-type and *Sell*$^{-/-}$ B cells. CD19$^+$ and CD138$^+$ cells are gated and their percentages are shown (G and I).

Data are representative from three (A–D and F) or two (E and G–I) independent experiments. See also Figure S2.